Published in final edited form as:

Mol Cell. 2021 October 21; 81(20): 4228–4242.e8. doi:10.1016/j.molcel.2021.09.024.

Aberrant RNA methylation triggers recruitment of an alkylation repair complex

Ning Tsao[1,^], **Joshua R. Brickner**[1,^], **Rebecca Rodell**[1], **Adit Ganguly**[1], **Matthew Wood**[2,3], **Clement Oyeniran**[1], **Tanveer Ahmad**[4], **Hua Sun**[1], **Albino Bacolla**[5], **Lisheng Zhang**[6], **Valentina Lukinović**[4], **Jennifer M. Soll**[1], **Brittany A. Townley**[1], **Alexandre G. Casanova**[4], **John A. Tainer**[5,7], **Chuan He**[6,8], **Alessandro Vindigni**[2], **Nicolas Reynoird**[4], **Nima Mosammaparast**[1,*]

[1]Department of Pathology & Immunology, Washington University in St. Louis School of Medicine, St. Louis, MO 63110, USA.

[2]Division of Oncology, Department of Medicine, Washington University in St. Louis School of Medicine, St. Louis, MO 63110, USA.

[3]Edward A. Doisy Department of Biochemistry and Molecular Biology, Saint Louis University School of Medicine, St. Louis, MO 63104, USA.

[4]Institute for Advanced Biosciences, Grenoble Alpes University, CNRS UMR5309, INSERM U1209, Grenoble, France.

[5]Department of Molecular and Cellular Oncology, University of Texas M.D. Anderson Cancer Center, Houston, TX 77030, USA.

[6]Department of Biochemistry and Molecular Biology, Department of Chemistry, and Institute for Biophysical Dynamics, The University of Chicago, Chicago IL 60637, USA.

[7]Molecular Biophysics and Integrated Bioimaging, Lawrence Berkeley National Laboratory, Berkeley, CA 94720, USA.

[8]Howard Hughes Medical Institute, The University of Chicago, Chicago IL 60637, USA.

Summary

Central to genotoxic responses is their ability to sense highly specific signals to activate the appropriate repair response. We previously reported that the activation of the ASCC-ALKBH3

[*]Lead contact: Nima Mosammaparast, Department of Pathology & Immunology, Washington University School of Medicine, 4940 Parkview Place, CSRB Room 7750, St. Louis MO, 63110, Telephone: 314-747-5472, nima@wustl.edu.

[^]These authors contributed equally

Author Contributions

N.T., J.R.B., R.R., A.G., M.W., C.O., T.A., V.L., J.M.S., B.A.T., A.G.C., and N.M. carried out cellular and biochemical experiments. H.S., A.B., and L.Z. performed RNA-Seq and CLIP-Seq bioinformatic analysis. J.A.T. supervised A.B. C.H. supervised L.Z. A.V. supervised M.W. N.R. supervised V.L., T.A., and A.G.C. N.M. supervised the project and wrote the manuscript with N.T. and J.R.B., with input from all other authors.

Declaration of Interests

The authors declare no competing financial interests.

repair pathway is exquisitely specific to alkylation damage in human cells. Yet the mechanistic basis for the selectivity of this pathway was not immediately obvious. Here, we demonstrate that RNA but not DNA alkylation is the initiating signal for this process. Aberrantly methylated RNA is sufficient to recruit ASCC, while an RNA dealkylase suppresses ASCC recruitment during chemical alkylation. In turn, recruitment of ASCC during alkylation damage, which is mediated by the E3 ubiquitin ligase RNF113A, suppresses transcription and R-loop formation. We further show that alkylated pre-mRNA is sufficient to activate RNF113A E3 ligase *in vitro* in a manner dependent on its RNA binding Zn-finger domain. Together, our work identifies an unexpected role for RNA damage in eliciting a specific response to genotoxins.

eTOC Blurb

Tsao et al. demonstrate that RNA and not alkylation is necessary and sufficient to recruit the ASCC-ALKBH3 damage repair complex. The ASCC pathway suppresses transcription and R-loop accumulation in response to alkylation stress. This E3 ubiquitin ligase activity of RNF113A, which recruits this complex, is induced by alkylated RNA.

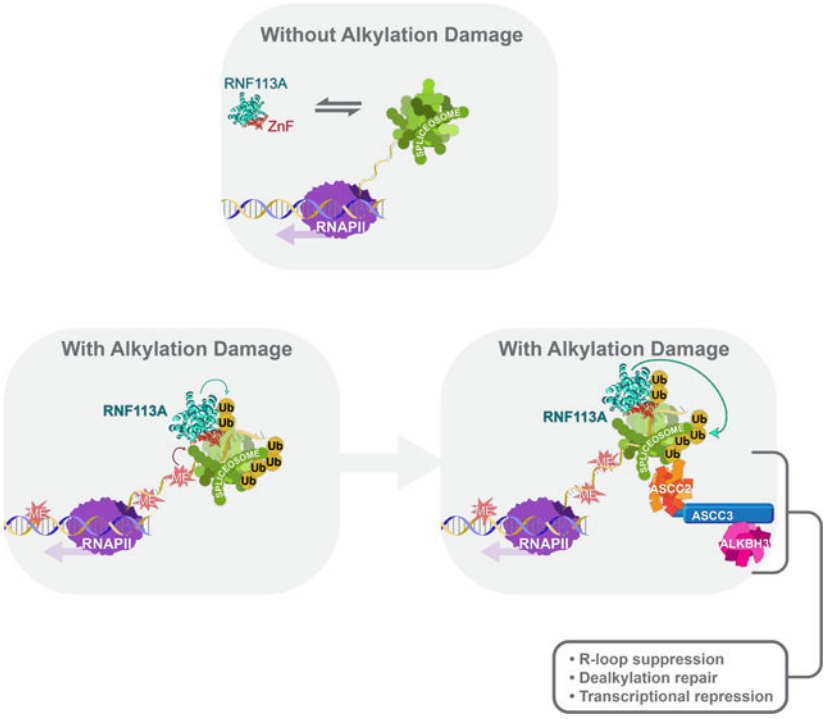

Introduction

The importance of genome maintenance is underscored by the evolution of multiple mechanisms to repair specific types of damaged DNA. Repair of alkylated DNA is particularly critical in cancer, since alkylation chemotherapy is used to treat many tumors (Fu et al., 2012; Soll et al., 2017). Alkylated bases can disrupt canonical base pairing, inhibit replication or induce mutagenesis (Fu et al., 2012; Soll et al., 2017). At least three major pathways are responsible for the repair of simple alkylated damage, including base excision repair, the AlkB family of demethylases, and methylguanine methyltransferase (Brickner et

al., 2019; Drablos et al., 2004; Fu et al., 2012). Evidence exists linking each pathway to alterations in alkylation damage responses in tumors (Butler et al., 2020; Fu et al., 2012; Soll et al., 2017). Yet it is unclear how any alkylation repair pathway is selectively activated, or how they are coordinated with other processes, such as transcription.

We previously showed that human ALKBH3 is coupled to the ASCC helicase, which is specifically recruited during alkylation damage to nuclear speckle bodies, corresponding to regions of RNA polymerase II transcript processing (Brickner et al., 2017). The recruitment of this complex requires K63-linked ubiquitination by the RNF113A E3 ubiquitin ligase and recognition of the ubiquitin chain by ASCC2. In a similar manner, the ASCC complex is also recruited to mediate ribosome quality control (RQC) (Juszkiewicz et al., 2020; Matsuo et al., 2020). Other established DNA damage signaling pathways, such as DNA double-stranded break repair, also depend on K63-linked ubiquitination (Schwertman et al., 2016). However, the molecular basis for the alkylation damage specificity in the RNF113A-ASCC-ALKBH3 pathway remains unclear.

Alkylating agents damage not only DNA, but also RNA (Fedeles et al., 2015; Vagbo et al., 2013). In fact, treatment of *E. coli* with the alkylating agent methyl methanesulfonate (MMS) resulted in 10-fold more alkylated lesions in RNA than DNA (Vagbo et al., 2013). Alkylated mRNAs likely induce various RNA degradation pathways, particularly RQC (Yan et al., 2019). Intriguingly, RNA dealkylation mechanisms exist, and some AlkB proteins are capable of repairing m1A and m3C in both single-stranded DNA and RNA (Aas et al., 2003; van den Born et al., 2008). RNA dealkylation has also been demonstrated for certain human AlkB proteins, including ALKBH1, ALKBH3, and ALKBH8 (Aas et al., 2003; Li et al., 2017; Liu et al., 2016; Ueda et al., 2017; van den Born et al., 2011). Emerging from these studies is the notion that alkylated RNA is likely to affect cellular physiology and mechanisms appear to have evolved to repair or remove damaged RNA.

Here, we demonstrate that aberrant RNA methylation activates the RNF113A-ASCC pathway. Interestingly, recruitment of ASCC mediates transcriptional downregulation and R-loop suppression. We further find that RNF113A E3 ligase activity is induced specifically during methylation damage, but not with other types of genotoxic agents. Mechanistically, we reveal that upon alkylation, RNF113A recognizes nascent pre-mRNAs in the context of the spliceosome, and that its E3 activity is induced by alkylated RNA through its ZnF domain. Our findings uncover a role for aberrantly methylated RNA in initiating the cellular response to alkylation via the activation of the RNF113A-ASCC pathway.

Results

RNA alkylation is necessary and sufficient to mediate ASCC recruitment

We previously reported the discovery of a nuclear signaling pathway that recruits the ASCC complex as part of the alkylation damage response (Brickner et al., 2017). Although the mechanistic basis for this alkylation damage selectivity was unclear, we reasoned that RNA modification may play an important role for such specificity. To test whether RNA damage was necessary for ASCC recruitment, we used an RNA-specific repair enzyme to counter the RNA alkylation without affecting DNA alkylation. We cloned

and characterized an AlkB demethylase from blueberry scorch disease virus (BsV), an RNA virus (van den Born et al., 2008). By using quantitative LC-MS/MS, we confirmed that BsV-AlkB can demethylate a m1A-modified RNA oligonucleotide but not a DNA substrate with the identical sequence (Figure 1a; Supplemental Figure S1a–S1c). Having established its selectivity for RNA, we expressed BsV-AlkB as an NLS-fusion in U2OS cells, which targeted it to the nucleus (Supplemental Figure S1d). Strikingly, BsV-AlkB-NLS expression significantly reduced HA-ASCC2 foci formation to background levels following MMS-induced alkylation damage (Figure 1b–c). The enzymatic activity of BsV-AlkB was important for foci suppression, as the H156A catalytic mutation was less capable of countering ASCC2 recruitment, indicating that RNA alkylation is necessary for MMS-induced ASCC2 foci formation.

To test if RNA methylation was sufficient to recruit the ASCC complex, we cloned the METTL8 methyltransferase, which produces 3-methylcytosine (m3C) on various RNAs (Xu et al., 2017). While the function of this modification is not fully clear, it is one of the major modifications produced on RNA by alkylating agents also a substrate for the AlkB enzymes (Aas et al., 2003; Drablos et al., 2004; Ougland et al., 2004). We purified METTL8 and various catalytic mutants from 293T cells (Supplemental Figure S2a–S2b). Using LC-MS/MS METTL8 was found to be active only on a ssRNA substrate *in vitro*; no activity was found on the same ssDNA substrate (Figure 2a–2b). We then expressed a human METTL8-NLS fusion, which was targeted to the nucleus, where it appeared to partition to the nucleolus (Supplemental Figure S2c). Ectopic expression of wildtype METTL8-NLS induced recruitment of the ASCC3 helicase to nucleolar regions (Figure 2c–2d). Conversely, two catalytic mutations targeting the putative SAM-binding domain of METTL8 (D'Silva et al., 2011; Noma et al., 2011) (G204A/G206A and D230A; Supplemental Figure S2a–S2c) failed to recruit ASCC3 to nucleoli (Figure 2c–2d and Supplemental Figure S2d). Using quantitative LC-MS/MS, we confirmed that these two METTL8 mutants were deficient for *in vitro* RNA methyltransferase activity (Figure 2a–2b). To provide further support for our model, we took advantage of a distinct RNA methyltransferase TRMT61A, which produces m1A – another substrate for the AlkB enzymes (Safra et al., 2017). NLS-fused TRMT61A was not present in nucleoli but instead localized to nuclear speckle bodies, marked by the spliceosomal protein PRP8 (Supplemental Figure 2e–2f), which coincides with the region to which ASCC is recruited during chemical alkylation (Brickner et al., 2017). Similar to METTL8, TRMT61A also resulted in recruitment of ASCC3 to these same regions in a manner that depended on the TRMT61A catalytic domain (Supplemental Figure S2g–S2h). In addition, TRM61A was able to recruit the ASCC-associated demethylase ALKBH3 (Supplemental Figure S2i–S2j) (Dango et al., 2011). However, TRMT61A expression was not capable of recruiting ALKBH2, suggesting specificity for the ASCC-ALKBH3 pathway (Supplemental Figure S2k).

During our analysis of METTL8-induced ASCC recruitment, we noted that the catalytically-inactive proteins failed to localize to nucleoli as robustly as the wildtype (Supplemental Figure S2c), which could alternatively explain impaired ASCC3 recruitment. To clarify this question, we utilized an inducible locus system where we could target this methyltransferase to an MS2-containing gene reporter (Janicki et al., 2004; Shanbhag et al., 2010). Here, fusing a degron-tagged METTL8-NLS to mCherry-LacI allowed for targeted recruitment

of the methyltransferase to the locus upon induction with the Shield1 ligand (Figure 2e). Although much of the WT protein still localized to nucleoli, METTL8 similarly induced ASCC3 recruitment to this locus, which in contrast was attenuated with the METTL8 G204A/G206A catalytic mutant (Figure 2f–g). Taken together, our results support the model that aberrant RNA methylation is both necessary and sufficient to recruit the ASCC complex.

Transcript and R-loop modulation by ASCC in response to alkylation damage

Previous work on ASCC has indicated that this complex can disassemble ribosomes stalled on mRNAs as part of RQC (Juszkiewicz et al., 2020; Yan et al., 2019). We reasoned that ASCC may function in analagously modulate transcription or promote RNA degradation during nuclear alkylation damage. RNA-Seq analysis revealed that while a global transcript downregulation did not occur in response to MMS, many mRNAs were altered under these conditions (Figure 3a and Supplemental Table 1). Notably, ASCC3 modulated differentially expressed genes (DEGs) upon MMS treatment; specifically, MMS-upregulated DEGs were modestly downregulated in ASCC3 KO cells (ΔLog2FC of −0.26 in WT vs. ASCC3 KO cells; Supplementary Figure S3a), whereas MMS downregulated DEGs were derepressed to a greater degree in ASCC3 KO cells (ΔLog2FC of +0.48 in WT vs. ASCC3 KO cells; Figure 3b and Supplemental Figure S3b). Thus ASCC3 potentially represses or degrades certain transcripts. Unabated transcription or lack of degradation of damage-associated transcripts may lead to R-loop accumulation, which could be detrimental for genomic integrity. Consistently, ASCC3 KO cells exhibited greater R-loops compared with controls upon MMS damage (Figure 3c). Since ASCC2 is a partner of ASCC3 and mediates targeting of ASCC3 (Brickner et al., 2017), we performed RNA-Seq in ASCC2 KO cells. Again, we found that loss of ASCC2 results in a signature that mirrors loss of ASCC3 during alkylation (Figure 3b and Supplemental Figure S3a–S3b). While loss of ASCC3 or ASCC2 did result in certain transcript changes in the absence of alkylation (Supplemental Figure S3c–d), functional analysis of these DEGs were not enriched for DNA repair or RNA processing (Supplemental Table 2). Thus, ASCC may have a direct role in R-loop suppression during alkylation stress.

To test if MMS-induced transcript alterations could be due to aberrant RNA methylation, we used the reporter system from Figure 2. Indeed, targeting METTL8 to this locus significantly reduced transcript levels from this reporter (Figure 3d–3f and Supplemental Figure S3e), which depended upon METTL8 methyltransferase activity (Figure 3d–3f). The deposition of m3C on the nascent transcript did not inhibit its quantitation by qRT-PCR; indeed, our results were not significantly altered after treatment of the purified RNA with ALKBH3 (Supplemental Figure S3f–3g), which preferentially demethylates m3C (Aas et al., 2003). To test whether loss of ASCC3 would alter the expression of nascent transcription from this reporter, we performed qRT-PCR upon ASCC3 knockdown (Supplemental Figure S3h–S3i). As with the global response to MMS seen by RNA-Seq, loss of ASCC3 partially derepressed this target locus. To determine whether this repression represented a general trend in response to nuclear RNA methylation, we expressed METTL8-NLS in WT and ASCC3 KO cells and analyzed transcription by RNA-Seq (Figure 3g and Supplemental Table 3). While the overall transcriptional changes were relatively modest in response to

METTL8-NLS compared to MMS treatment, we again found that loss of ASCC3 caused derepression of genes downregulated by METTL8-NLS (Figure 3g). Our data indicates that the ASCC complex is recruited to sites harboring aberrant RNA methylation to mitigate their expression or induce their turnover, in turn limiting R-loop formation.

To further delineate the mechanism of ASCC3 during alkylation, we created a homozygous knock-in mutation (ASCC3$^{G1354D/G1354D}$; designated ASCC3$^{KI/KI}$) previously reported to abolish its helicase activity (Dango et al., 2011) (Supplemental Figure S3j). RNA-Seq analysis revealed a preferential modulation of downregulated DEGs during alkylation, mirroring the ASCC3 KO (Figure 3h, Supplemental Figure S3k, and Supplemental Table 4). We focused on three genes, which we confirmed to be partially derepressed upon alkylation in ASCC3$^{KI/KI}$ cells (Supplemental Figure S3l). We then used ethynyl uridine (EU) labeling to isolate and analyze nascent transcripts; this showed that all three had modestly greater nascent transcript levels after MMS treatment in the ASCC3$^{KI/KI}$ than control cells (Figure 3j). A subsequent chase revealed little degradation of two of the three transcripts in control cells, while the third (HOXD11) exhibited ~50% loss after 3 hours. Notably, there was no significant difference at the end of the EU-chase in any of these transcripts in WT or ASCC3$^{KI/KI}$ cells (Figure 3k). These data indicate that the DNA helicase activity of ASCC3 may suppress nascent transcription during damage. Importantly, the ASCC3$^{KI/KI}$ cells also had a higher level of R-loop accumulation upon alkylation (Figure 3l), underscoring the functional significance of its activity during damage.

Selective activation of RNF113A E3 ligase upon alkylation damage

The above data indicated a role for RNA damage in ASCC recruitment. We reasoned that RNF113A, which acts upstream of ASCC, could be activated during alkylation. By using tandem ubiquitin binding element (TUBE) conjugated beads to isolate ubiquitinated proteins, we found that RNF113A was ubiquitinated in response to MMS, but not by other types of damaging agents (Figure 4a), despite the fact that they induced similar or greater levels of DNA damage signaling, as assessed by pH2A.X (Supplemental Figure S4a). Deletion or mutation of the RING domain significantly reduced RNF113A ubiquitination upon MMS treatment, indicating that this represents *bona fide* autoubiquitination (Supplemental Figure S4b). We then used different TUBE reagents that recognize ubiquitin chains non-specifically (Ubiquilin) or K63-linked chains (TAB2). This showed that a significant portion of the ubiquitin linkage associated with RNF113A activation was K63-linked, consistent with previous findings demonstrating that RNF113A functions with the K63-specific E2 enzyme UBC13 (Brickner et al., 2017) (Figure 4b). Equimolar concentrations of the methylating agent methyl iodide (MeI) induced autoubiqitination of RNF113A but the ethylating agent ethyl methanesulphonate (EMS) was significantly less potent in this assay, suggesting that RNF113A is preferentially activated by methylation compared to larger adducts, or that EMS is less reactive than MMS (Supplemental Figure S4c). Consistent with its autoubiquitination, RNF113A purified from cells pretreated with MMS was significantly more active as an E3 ligase compared to RNF113A purified from control cells; this *in vitro* result may represent ubiquitination of an associated, larger molecular weight protein (Figure 4c). MMS-induced autoubiquitination was specific to RNF113A, as RNF8 and RNF168, two E3 ligases involved in DNA damage signaling,

were not autoubiquitinated upon alkylation (Figure 4d), although alkylation induced RNF8/RNF168 recruitment to pH2A.X foci (Figure S4d). The recruitment of these E3s coincided with increased double-stranded DNA break signaling in S/G2 cells, as determined by pH2A.X foci formation in a FUCCI (fluorescence ubiquitin cell cycle indicator; (Sakaue-Sawano et al., 2008)) cell system (Supplemental Figure S4e), likely representing replication-dependent DNA breaks.

To further probe the mechanism of RNF113A activation, we expressed the BsV-AlkB protein prior to assessing RNF113A autoubiquitination. WT BsV-AlkB-NLS significantly reduced RNF113A autoubiquitination in two different cell lines, in contrast to the catalytic mutant, which was markedly attenuated in these assays (Figure 4e). This suggested that RNA alkylation may play a role in activating RNF113A. Indeed, expression of nuclear TRMT61A recruited ALKBH3 to nuclear speckles in a manner that was suppressed upon RNF113A depletion (Figure 4f and Supplemental Figure S4f). Loss of RNF113A resulted in markedly increased sensitivity to MMS but not camptothecin, as determined by a colorimetric survival assay and a colony formation assay (Figure 4g and Supplemental Figure S4g–i). This increased sensitivity to MMS was not rescued by BsV-AlkB expression; thus, RNA damage repair alone likely does not account for this MMS hypersensitivity (Supplemental Figure S4j–k). Indeed, loss of ALKBH3, which demethylates both RNA and DNA, was epistatic with RNF113A loss (Figure 4h and Supplemental Figure S4l). To directly determine whether RNF113A promotes DNA alkylation reversal, we analyzed 1meA repair using quantitative mass spectrometry. This demonstrated a modest but significant increase in the amount of retained 1meA upon loss of RNF113A during recovery from MMS damage (Figure 4i). Importantly, neutral comet assays also revealed a greater number of DNA breaks during recovery from alkylation damage in RNF113A depleted cells (Figure 4j). Altogether, these data indicate that while RNF113A is activated primarily upon RNA alkylation, it plays a vital role in DNA alkylation reversal and genomic integrity.

RNF113A activation as part of the spliceosome

RNF113A appears to be specifically activated in response to alkylation damage, but the molecular mechanism for this activation is not understood. Structural studies on RNF113A and its yeast orthologue Cwc24p have demonstrated spliceosomal association (Haselbach et al., 2018; Yan et al., 2016). Specifically, the CCCH-type zinc-finger associates with the 5′ splice site of pre-mRNAs in the active spliceosome (Figure 5a and Supplemental Figure S5a–S5b). RNF113A may therefore function to interrogate pre-mRNA integrity. To further analyze the relationship between RNF113A and the spliceosome during alkylation, we performed a proteomic analysis of RNF113A interactors in HeLa-S cells before and after MMS treatment (Figure 5b, Supplemental Figure S5c, and Supplemental Table 5). RNF113A was associated with spliceosomal components, and many of these interactions, such as with the spliceosomal protein BRR2/SNRNP200, as well as SR proteins, were increased after MMS damage; associations with proteins involved in other pathways, such DNA repair (RIF1) or translation initiation (EIF4B) were also induced with MMS. Co-immunoprecipitation verified the MMS-induced RNF113A interaction with SRRM2 and BRR2, which were resistant to benzonase treatment (Figure 5c). These data suggested that RNF113A E3 activation may be linked to a more stable association with the spliceosome

when it encounters damaged RNA. We reasoned that if we inhibit spliceosome activity at a step prior to RNF113A binding, MMS-induced activation of this E3 would be mitigated. Addition of a small molecule inhibitor PB, which binds to SF3B and inhibits early spliceosome activation (Cretu et al., 2018) reduced MMS-mediated RNF113A autoubiquitination, while significantly increasing pH2A.X signaling (Figure 5d). This potentially links spliceosomal function, RNF113A activation, and DNA damage signaling.

To complement these studies, we performed RNA-immunoprecipitation followed by mass spectrometry (RIP-MS) of nucleotides, resulting from RNase treatment, from cells expressing Flag-RNF113A. Upon MMS treatment, association between RNF113A and RNA increased significantly (Figure 5e). More importantly, our tandem MS analysis allowed us to interrogate whether these RNAs included alkylated ribonucleosides. MMS-induced modifications m1A, m3C, and m7G were associated with RNF113A-bound RNAs (Figure 5f). Cross-linked immunoprecipitation followed by deep sequencing (CLIP-Seq) confirmed that RNF113A interacted primarily with pre-mRNAs (67.6%), with nearly half of these interactions (47.9%) occurring in intronic regions, although additional high-confidence CLIP hits were also identified (Figure 5g–5h and Supplemental Table 6). Altogether, these data supported the model that RNF113A E3 activation may be linked to a more stable association with the spliceosome, where it may encounter damaged RNA.

Direct activation of RNF113A E3 ligase by methylated RNA

The ASCC complex is recruited by methylation of RNA, and RNF113A is activated and recruited to the spliceosome during alkylation, implying that RNF113A E3 ligase activity may be stimulated by damaged pre-mRNA. We therefore used RNF113A complex purified from HeLa-S nuclear extracts and tested the ability of damaged RNAs to induce its E3 activity. We first used *in vitro* transcribed β-globin pre-mRNA (Movassat et al., 2014) as a potential substrate for inducing RNF113A E3 activity. While the unmodified RNA had a mild stimulatory effect on the E3 activity of RNF113A, we observed a marked increase in the E3 activity when the same RNA was pre-methylated *in vitro* (Figure 6a). LC-MS/MS validated the presence of methylated RNAs including m7G, m1A, and m3C (Supplemental Figure S6a); in addition, the alkylated form of this RNA appeared less capable of splicing *in vitro* (Supplemental Figure S6b). The modified RNA alone lacked any apparent E3 activity, suggesting a stimulation of RNF113A (Supplemental Figure S6c). We then assessed whether an RNA oligonucleotide bearing a specific methylation mark was capable of increasing the E3 activity of RNF113A. As many of these damage-induced modifications, such as m7G, are relatively unstable, only m1A-containing oligonucleotides were commercially available. A single-stranded RNA oligo containing an m1A modification, but not its unmodified counterpart, induced the E3 activity of RNF113A (Figure 6b). In contrast, the identical DNA oligonucleotide containing 1-methyldeoxyadenosine at the same position had no apparent effect on increasing ubiquitination by RNF113A (Figure 6b). Thus, RNF113A appears to encode an E3 ligase that is responsive to RNA damage.

The presence of a conserved RNA-binding ZnF (Figure 5a) suggested that this region of RNF113A may act in its association with pre-mRNAs upon alkylation. To test this, we created two site-directed mutants within this domain. RIP-MS from cells expressing these

mutant forms of RNF113A demonstrated a reduced degree of MMS-induced RNA binding relative to WT RNF113A (Figure 6c and Supplemental Figure S6d). To determine the functional significance of this binding, we focused on the K218A/F219A mutant. Notably, this mutant still localized to nuclear speckle bodies, as with WT RNF113A, suggesting that this protein is properly folded (Supplemental Figure S6e). However, compared to WT RNF113A, the mutant was markedly less capable of MMS-induced association with BRR2 (Supplemental Figure S6f), In addition, it had a markedly reduced ability to be activated by MMS, as assessed by autoubiquitination via TUBE assay (Figure 6d). We then tested the ability of the m1A-containing oligonucleotide to activate the K218A/F219A mutant. In contrast to WT RNF113A, the E3 ligase activity of the K218A/F219A mutant appeared increased at baseline but was not further activated by the m1A-containing RNA (Figure 6e). To test the function of this mutant in cells, we performed knockdown-rescue experiments and assayed for MMS-induced ASCC3 foci formation in U2OS cells (Figure 6f and Supplemental Figure S6g). Expression of WT RNF113A rescued ASCC3 foci formation; however, the K218A/F219A mutant did not, implying that the ZnF domain is important for RNF113A function during alkylation damage. As with loss of ASCC3, MMS-induced R-loop accumulation was exacerbated by RNF113A loss (Figure 6g and Supplemental Figure S7h). While WT RNF113A expression reduced R-loop accumulation under these conditions, the K218A/F219A mutant was defective in this respect. Consistent with these phenotypes, cells expressing the ZnF domain mutant were sensitive to MMS to nearly the same degree as RNF113A lacking its catalytic RING finger domain (Figure 6h). Altogether, these data indicate a functional role of the RNA binding ZnF domain of RNF113A in activation of its E3 ligase activity, which in turn promotes ASCC3 recruitment and alkylation damage resistance.

Discussion

Although relatively unexplored, recent work has begun to highlight the importance of RNA in propagating genotoxic responses, particularly for promoting homologous recombination, microhomology mediated repair, and non-homologous end joining during double-strand break repair (Bader et al., 2020; Mazina et al., 2017). While these studies have focused on the role of RNA-associated proteins, transcripts and R-loops in mediating repair, our study highlights a mechanism by which aberrant RNA methylation activates a signaling response to recruit the ASCC complex, which in turn helps to maintain the genome. While these “aberrant” methylations are strongly induced by alkylating agents, we should note that they are thought to exist in certain mRNAs, albeit in low amounts under normal cellular conditions, such as internal m7G sites within certain mRNAs (Zhang et al., 2019), which may in turn activate this pathway. Thus, it is plausible that even in unperturbed cells, this pathway is nominally responding to repair alkylated bases that may be induced inappropriately through off-target effects of these methyltransferases. Indeed, basal RNF113A activity in the absence of exogenous damage may allow the pathway to be activated quickly in response to such endogenous events.

How cells shut down transcription, both locally and globally, in response to DNA damage is an area of increasing interest. Here, we show that aberrant methylation damage, either by alkylating agents such as MMS or overexpression of METTL8, results in repression

of certain target genes (Figure 3). These alkylation-repressed transcripts are partially derepressed upon loss of either ASCC3 or ASCC2. Such findings support and extend previous results that suggest that the ASCC complex shuts down nascent transcription globally upon UV damage (Williamson et al., 2017). It is likely that this activity of the ASCC complex is responsible for suppressing R-loops upon alkylation stress.

Consistent with previous findings, we demonstrate that RNF113A E3 ligase activity is specifically stimulated by alkylation damage (Figure 4). Loss of RNF113A sensitized cells to alkylation damage, but not to other DNA damaging agents, mirroring our previous results with the ASCC complex (Brickner et al., 2017). This phenomenon appears to be specific to this alkylation repair pathway, as MMS did not significantly induce the autoubiquitination of RNF8 or RNF168, two well-characterized ligases involved in double-strand break repair (Schwertman et al., 2016). Notably, these latter E3 ligases appear to be regulated primarily by recruitment to sites of DNA double-stranded break-induced foci, which are also induced by MMS primarily in S/G2 phase of the cell cycle, whereas RNF113A is constitutively associated with nuclear speckle bodies.

In concert with prior published data, our results here suggest a working model for how RNF113A functions upstream of the ASCC complex in response to alkylation stress (Figure 7). RNF113A associates transiently with the active spliceosome, but this association is stabilized upon alkylation damage. Our data indicate that RNF113A interacts with damaged RNA through its ZnF domain; however, as depicted in our first working model (Figure 7a), it is unlikely that this domain directly recognizes a specific modification on the RNA. While we cannot rule out the possibility that this ZnF domain recognizes methylated nucleotides directly (Figure 7b), we have not observed a stable interaction between RNF113A and alkylated RNA (data not shown). Thus, we reason that alkylated RNA, which we find inhibits pre-mRNA processing on the spliceosome, may in turn be the signal to recruit and activate the RNF113A E3 ligase. In either case, this association of RNF113A culminates in its autoubiquitination as well as ubiquitination of other proteins in the spliceosome, such as BRR2 (Brickner et al., 2017). In turn, the K63-linked ubiquitination recruits the ASCC complex via the ASCC2 subunit. The recruitment of ASCC by RNF113A mediates repression of nascent transcription and prevents R-loop accumulation.

Our previous findings indicate that ASCC-ALKBH3 functions as a complex (Dango et al., 2011; Brickner et al., 2017), whose loss impairs repair kinetics of alkylated lesions in DNA. RNF113A also promotes more efficient repair of DNA double-stranded breaks secondary to alkylation damage (Figure 4); consistently, expression of the RNA selective BsV-AlkB protein does not rescue the alkylation damage sensitivity of RNF113A deficiency. Combined with our evidence that RNF113A is epistatic to ALKBH3, these data indicate that RNF113A promotes alkylation damage reversal on DNA. Yet, as alkylated RNA is more abundant, having the initial pathway activation signal through RNA may have evolved as a more sensitive mechanism to detect and indicate alkylation damage in the nucleus. The fact that ALKBH3 can repair both ssRNA and ssDNA (Aas et al., 2003; Sundheim et al., 2006), and the ability of ASCC3 to unwind DNA (Dango et al., 2011) and also function in RQC further bolsters the multifunctionality of this complex in repairing or ridding cells of damaged RNA as well as DNA. Therefore, our work has potentially unveiled the adaptation

of RNA damage recognition as a mechanism to recruit the ASCC complex to damaged, transcriptionally active regions to maintain genomic integrity.

Limitations of the study

Our work strongly suggests that the ASCC complex utilizes its helicase activity to downregulate nascent transcription and suppress R-loop formation, yet how it would use its motor activity to this end is unclear. Furthermore, our findings establish a major mechanism by which RNF113A is directly activated as an E3 ligase by alkylated RNA, which to our knowledge has yet to be described in the literature. However, the precise mechanism by which damaged RNA activates this E3 ligase is unknown. In addition, we cannot rule out other mechanisms that act upstream of RNF113A to regulate its E3 ligase activity. Indeed, many E3 ligases are regulated by other post-translational modifications (Song and Luo, 2019). Structural studies will likely be necessary to fully understand its regulation and mechanism of action.

STAR Methods

RESOURCE AVAILABILITY

Lead Contact—Further information and requests for resources and reagents should be directed to and will be fulfilled by the Lead Contact, Nima Mosammaparast (nima@wustl.edu).

Materials Availability—All reagents generated in this study are available from the Lead Contact without restriction.

Data and Code availability

- RNA-seq data have been deposited at GEO and are publicly available as of the date of publication. Accession numbers are listed in the key resources table. Original western blot and microscopy image data have been deposited at Mendeley and are publicly available as of the date of publication. The DOI is listed in the key resources table.
- This paper does not report original code.
- Any additional information required to reanalyze the data reported in this paper is available from the lead contact upon request.

EXPERIMENTAL MODEL AND SUBJECT DETAILS

Cell culture—Human cell lines (293T, HeLa, HeLa-S, and U2OS; all originally from ATCC) were cultured in Dulbecco's modified eagle medium (Invitrogen), supplemented with 10% fetal bovine serum (Sigma), 100 U/ml of penicillin-streptomycin (Gibco) at 37°C and 5% CO_2. U2OS FUCCI contains integrated lentiviral mKO2-hCdt1 and mAG-hGem cell cycle reporters (Byrum et al., 2019). The U2OS ASCC3 KO and U2OS ASCC2 KO cell lines contain CRISPR/Cas9 derived mutations that render each respective locus as homozygous null (Brickner et al., 2017). U2OS 2–6–3 cell line contains tet-inducible, CMV minimal promoter reporter cassettes expressing MS2 repeats at chromosome 1 (Janicki

et al., 2004; Shanbhag et al., 2010). The U2OS ASCC3$^{KI/KI}$ mutant cell line contains a homozygous mutation encoding the G1354D substitution in *ASCC3*.

METHOD DETAILS

Plasmids—Plasmids containing human ASCC2 and RNF113A cDNAs were previously described (Dango et al., 2011). The BsV-AlkB cDNA (van den Born et al., 2008) was synthesized as a gBlock (IDT) after optimization of the sequence for human cell expression, fused to the SV40 NLS, and cloned into pENTR3-C. METTL8 was amplified from human cDNA, fused to the SV40 NLS, and cloned into pENTR-3C. TRMT61A cDNA was synthetically generated (GenScript), fused to SV40 NLS and cloned into pENTR-3C. For mammalian cell expression, cDNAs were subcloned into pHAGE-CMV-3xHA, pHAGE-CMV-Flag, pMSCV (no tag), or pMSCV-Flag-HA as needed by Gateway recombination (Brickner et al., 2017). For degron tagged expression, the mCherry-LacI sequence (from Addgene #18985) was subcloned into pLVX-PTuner (Takara Bio). To create the DD-Flag-METTL8-NLS-mCherry-LacI, Flag-METTL8-NLS was subcloned into the pLVX-PTuner-mCherry-LacI. For recombinant protein expression, cDNAs were subcloned into pET28a-Flag. Mutations were created by PCR-mediated mutagenesis or synthesized as gBlocks (IDT). For shRNA-mediated knockdowns, TRC pLKO.1 vectors were used as previously described (Brickner et al., 2017). For CRISPR/Cas9 mediated knockout of RNF113A, gRNA sequences were cloned into pLentiCRISPR-V2 (Addgene#52961). The T7 β-globin minigene construct for *in vitro* transcription of β-globin pre-mRNA was kindly provided by Dr. Klemens Hertel (University of California, Irvine), and was described previously (Movassat et al., 2014). All constructs derived by PCR or from gBlocks were confirmed by Sanger sequencing.

Cell culture and cell survival assays—The U2OS FUCCI cell line (Byrum et al., 2019) and the ASCC2 and ASCC3 knockout cell lines (Brickner et al., 2017) were previously described. The U2OS 2–6-3 reporter cell line (Janicki et al., 2004; Shanbhag et al., 2010) was a kind gift of Roger Greenberg (University of Pennsylvania). The ASCC3$^{G1354D/G1354D}$ knock-in cell line was created using CRISPR/Cas9 and homologous recombination of a donor DNA containing the desired mutation at the Washington University GEiC core facility. Clones were screened and verified by deep sequencing. Preparation of viruses, transfection, and viral transduction were performed as described previously (Brickner et al., 2017). Knockdown experiments (using shRNA) and knockout experiments (using CRISPR/Cas9) were performed by infecting cells with the indicated lentivirus and selecting with puromycin (1 μg/ml) for 48–72 hours. For ASCC foci rescue experiments, cells were transduced with the indicated pMSCV retroviral vector. For DNA damaging agent survival assays using HeLa cells, 1500–2000 cells per well were cultured overnight in 96-well plates in 100 μl media. Cells were then exposed to medium containing the indicated concentration of methyl methanesulphonate (MMS; Sigma) for 24 hours at 37 °C. The media was then replaced with normal media, and cell viability was assessed using the MTS assay (Promega) 72 hours after initial damaging agent exposure. For experiments involving camptothecin (CPT; Sigma), cells were exposed to medium containing the indicated concentration of the damaging agent in culture medium for 72 hours at 37 °C. Viability was then processed by MTS assay as above. All MTS-based survival experiments

were carried out in technical quintuplicate. For colony formation assay, knockout or control HeLa cells were trypsinized, counted, and plated at low density. After overnight incubation, the cells were treated with the indicated doses of MMS or camptothecin for 24 hours in complete medium. The cells were incubated for 12–14 days, fixed, and stained with crystal violet. The experiment was performed in quadruplicate for each cell line and drug dose. Colonies were counted and relative survival was normalized to untreated controls.

Neutral comet assay—HeLa cells were plated 24 hours before treatment with 0.5 mM MMS for 1 hour. Media was replaced and incubated for another two hours when indicated. Cells were then trypsinized and resuspended to 3 X 10^5 cells/mL in cold PBS. Neutral comet assays were performed using CometAssay (Trevigen), according to manufacturer's protocol. Cells were combined with low melting point agarose 1:10 and spread onto a comet slide (Trevigen) and allowed to dry at 4°C for 30 minutes. Slides were placed in lysis solution (Trevigen) at 4°C for 1 hour before immersion in 1X TBE (0.1M Tris Base, 0.1M Boric Acid, 2.5mM EDTA) for 30 minutes. Lysed cells were then electrophoresed at 25V for 30 minutes at 4°C. Slides were incubated with DNA precipitate solution (1M Ammonium Acetate, 95% EtOH) for 30 minutes, and subsequently incubated in 70% EtOH for 30 min. Slides were then dried overnight at room temp. Slides were stained with 1X SYBR Gold (Thermo Fisher) for 30 min, and images were acquired with a fluorescence microscope (LEICA DMU 400B; 10X). At least 75 comets were scored for each condition using OpenComet in ImageJ software.

Protein purification—Recombinant, His-tagged BsV-AlkB and ALKBH3 proteins were purified from Rosetta (DE3) cells using an ÄKTA-pure FPLC (GE Healthcare). Cells were resuspended in His-lysis buffer (50 mM Tris-HCl pH 7.3, 250 mM NaCl, 0.05% Triton X-100, 3 mM β-ME, 30 mM imidazole, and protease inhibitors) and lysed by sonication. After centrifugation and filtration, the extract was loaded onto a HisTrap HP column using a 50 ml Superloop (GE Healthcare). After extensive washing with lysis buffer, the protein was eluted using lysis buffer containing 400 mM imidazole. All recombinant proteins were dialyzed into TAP buffer. Flag-tagged METTL8 was purified from transiently transfected 293T cells by resuspension in Flag-lysis buffer (50 mM Tris-HCl pH 7.9, 150 mM NaCl, 10% glycerol 1.0% Triton X-100, 1 mM DTT, and protease inhibitors) and lysed by sonication. After incubation with Flag resin, beads were washed three times with 10 ml of Flag-lysis buffer and twice with 4 ml Flag-lysis buffer. The protein was eluted with TAP wash buffer (50 mM Tris, pH 7.9, 100 mM KCl, 5 mM $MgCl_2$, 0.2 mM EDTA, 0.1% NP-0, 10 % glycerol, 2 mM DTT) containing 0.4 mg/ml Flag peptide.

RNF113A complex purification and proteomic analysis—Flag-HA-RNF113A was stably expressed after transduction of pMSCV-Flag-HA-RNF113A retrovirus into HeLa-S cells. Nuclear extract was prepared from the stable cell line with or without prior treatment with MMS (0.5 mM for 30 minutes for IP-MS, 5 mM for 1 hour for IP-Western), and the RNF113A complex was purified using anti-Flag (M2) resin (Sigma) in TAP buffer (50 mM Tris-HCl pH 7.9, 100 mM KCl, 5 mM $MgCl_2$, 10% glycerol, 0.1% NP-40, 1 mM DTT, and protease inhibitors). For benzonase treatment, EDTA was omitted from TAP buffer and 100 U/ml benzonase was added into the cell lysates prior to the immunoprecipitation. After

peptide elution, the complexes were subjected to Western blotting with indicated antibodies or TCA precipitated and associated proteins were identified by LC-MS/MS at the Taplin Mass Spectrometry Facility (Harvard Medical School) using an LTQ Orbitrap Velos Pro ion-trap mass spectrometer (ThermoFisher) and Sequest software (Eng et al., 1994). Total and unique peptide spectral counts, as well as total peptide intensities, can be found in Supplemental Table 5.

Alkylated pre-mRNA preparation—*In vitro* transcription of β-globin pre-mRNA was performed by using HiScribe T7 *In Vitro* Transcription Kit (NEB). The *in vitro* transcribed pre-mRNA was treated with dimethyl sulfate (DMS) as described (Tijerina et al., 2007). RNA was added into a 25 μl reaction mixture containing 0.65% DMS, 50 mM Na-MOPS pH 7.0, 10 mM $MgCl_2$, and incubated at room temperature for 10 minutes. Reactions were quenched with 475 μl quench solution (0.3 M sodium acetate, 30% β-Mercaptoethanol) prior to ethanol precipitation. The RNA pellets were dissolved in water and concentration was determined using a Nanodrop. Methylation status of the ribonucleosides was analyzed by quantitative LC-MS/MS, as described below.

Nucleic acid demethylase and methyltransferase assays—For demethylation assays, methylated oligonucleotides (RNA and DNA sequences shown in Key Resources Table) were purchased from Midland Certified Reagents Company (Midland, TX). Demethylation reactions were carried out using 60 pmol of substrate oligonucleotide in the presence of 20 pmol BsV-AlkB protein for 1 hour at 37°C in a 50 μl reaction mixture containing 50 mM HEPES–KOH pH 7.5, 2 mM ascorbic acid, 100 μM 2-oxoglutarate, 40 μM $FeSO_4$ and 1 ul RNaseOUT recombinant ribonuclease inhibitor (ThermoFisher). Methyltransferase assays were carried out using 100 pmol of substrate oligonucleotide (IDT; see Key Resources Table for sequence) in the presence of ~0.5μg of immunopurified Flag-METTL8 for 2 hours at 37°C in a 40 μl reaction mixture containing 50 nM HEPES pH 7.5, 3 mM $MgCl_2$, 0.5 mM S-adenosylmethonine and 1 μl RNaseOUT recombinant RNase inhibitor. The products for both types of reactions were digested to nucleosides and analyzed by quantitative LC-MS/MS, as described below.

RNA immunoprecipitation (RIP) for LC-MS/MS analysis—The procedure was followed as previously described (Wang et al., 2014), with minor modifications. HeLa-S cells expressing empty pMSCV-Flag vector, Flag-RNF113A (WT), or ZnF point mutants grown in 15-cm dishes were treated with or without 5 mM MMS for 1 hour. Cells were harvested and the pellets were lysed with 2 volumes of lysis buffer (10 mM HEPES pH 7.5, 150 mM KCl, 0.5% NP-40, 2mM EDTA, 0.5mM $Zn(NO_3)_2$, 10 mM β-ME, protease inhibitors and 400 U/ml RNase inhibitor), incubated on ice for 5 minutes then shock-frozen at - 80°C for 30 minutes. Cell lysates were thawed on ice and centrifuged at 15,000g for 15 minutes. The supernatant was immunoprecipitated with M2 agarose beads at 4°C for 4 hours. Beads were washed eight times with 1 ml ice-cold NT2 buffer (50 mM HEPES pH 7.5, 200 mM NaCl, 0.05% NP-40, 2mM EDTA, 0.5mM $Zn(NO_3)_2$, 10 mM β-ME and 200 U/ml RNase inhibitor) and eluted with 5 packed bead volumes of NT2 buffer containing 0.4 mg/ml Flag peptide. The supernatant was mixed with 1 ml TRIzol for RNA extraction

according to the manufacture's protocol, then digested for nucleoside mass spectrometry analysis.

Nucleoside Mass Spectrometry—With the exception of the analysis of genomic DNA after MMS treatment, samples were digested to nucleosides at 37°C overnight with Nuclease S1 from *Aspergillus oryzae* (Sigma-Aldrich), followed by dephosphorylation with FastAP alkaline phosphatase (Thermo Fisher) at 37°C for 1 hour. For genomic methylation adduct analysis, genomic DNA was extracted using using the DNeasy Blood & Tissue Kit (Qiagen). 5 μg genomic DNA was digested with Nucleoside Digestion Mix (NEB) at 37°C for 3 hours prior to LC-MS/MS analysis. Chromatographic separation was performed using an Agilent 1290 Infinity II UHPLC system with a ZORBAX RRHD Eclipse Plus C18 2.1 × 50 mm (1.8 um) column. The mobile phase consisted of water and methanol (with 0.1% formic acid) run at 0.5 ml/min. For DNA nucleosides, the run started with a 3 min gradient of 2–8% methanol, followed by a 2 min gradient of 8–98% methanol, 98% methanol was maintained for 4 min, followed by re-equillibration to 2% methanol over 1 min. For RNA nucleosides, the run started with a 3 min gradient of 2–8% methanol, followed by a sharp increase to 98% methanol which was maintained for 4 min. Mass spectrometric detection was performed using an Agilent 6470 Triple Quadrupole system operation in positive electrospray ionization mode, monitoring the mass transitions 266.13/150 (for m1dA), 252.11/136 (for dA), 282/150 (for m1A), 268.1/136 (for A), 242.1/126.1 and 242.1/109 (for m3dC), 228.1/112 (for dC), 258/126 (for m3C), 244.1/112 (for C), 298/166 (for m7G), and 284.2/152 (for G).

RNA Sequencing and Analysis—RNA was purified using the Qiagen RNeasy Mini Kit (#217004). Samples were prepared according to library kit manufacturer's protocol, indexed, pooled, and sequenced on an Illumina HiSeq. Basecalls and demultiplexing were performed with Illumina's bcl2fastq software and a custom python demultiplexing program with a maximum of one mismatch in the indexing read. RNA-seq reads were then aligned to the Ensembl release 76 top-level assembly with STAR version 2.0.4b(Dobin et al., 2013). Gene counts were derived from the number of uniquely aligned unambiguous reads by Subread:featureCount version 1.4.5(Liao et al., 2014). Isoform expression of known Ensembl transcripts were estimated with Salmon version 0.8.2 (Patro et al., 2017). Sequencing performance was assessed for the total number of aligned reads, total number of uniquely aligned reads, and features detected. The ribosomal fraction, known junction saturation, and read distribution over known gene models were quantified with RSeQC version 2.3 (Wang et al., 2012).

All gene counts were then imported into the R/Bioconductor package EdgeR(Robinson et al., 2010) and TMM normalization size factors were calculated to adjust for samples for differences in library size. Ribosomal genes and genes not expressed in the smallest group size minus one sample greater than one count-per-million were excluded from further analysis. The TMM size factors and the matrix of counts were then imported into the R/Bioconductor package Limma (Ritchie et al., 2015). Weighted likelihoods based on the observed mean-variance relationship of every gene and sample were then calculated for all samples with the voomWithQualityWeights (Liu et al., 2015). The performance of all genes

was assessed with plots of the residual standard deviation of every gene to their average log-count with a robustly fitted trend line of the residuals. Differential expression analysis was then performed to analyze for differences between conditions and the results were filtered for only those genes with Benjamini-Hochberg false-discovery rate adjusted *p*-values less than or equal to 0.05. For each contrast extracted with Limma, global perturbations in known Gene Ontology (GO) terms and KEGG pathways were detected using the R/Bioconductor package GAGE (Luo et al., 2009) to test for changes in expression of the reported $\log_2$ fold-changes reported by Limma in each term versus the background $\log_2$ fold-changes of all genes found outside the respective term. Heatmaps were generated using the Heatmapper online tool (heatmapper.ca). All RNA-Seq primary data and metadata have been deposited in the Gene Expression Omnibus repository (https://www.ncbi.nlm.nih.gov/geo) under accession number GSE158090.

qRT-PCR and nascent RNA analysis—For the MS2 reporter analysis, RNA was extracted using the Qiagen RNeasy Mini Kit (#217004). Reverse transcription was performed on the purified RNA with the ProtoScript First Strand cDNA Synthesis Kit (NEB E6300) using poly(dT) primers. SYBR Green JumpStart Taq Ready Mix (Sigma S9194) with used with qPCR using the QuantStudio 6 Flex Real-Time PCR System (Applied Biosystems). For nascent RNA analysis, cells were incubated with 0.2 mM 5-ethynyl uridine (EU) at 37°C for 1 hour, then harvested for total RNA extraction at indicated time points. 5 μg total RNA was subjected to nascent transcript isolation by using Click-iT Nascent RNA Capture Kit (Thermo Fisher Scientific, C10365). After reverse transcription, 1 μL cDNA from each sample was used for qPCR by using Power SYBR™ Green PCR Master Mix (Thermo Fisher Scientific) and QuantStudio 6 Flex Real-Time PCR System.

CLIP-Seq and Analysis—Ten 15-cm dishes of HeLa cells expressing pMSCV-Flag vectors were used for each CLIP. Cells were treated with 5 mM MMS for 1 hour and crosslinked by exposing twice with 0.15 J/cm^2 of 254 nm UV, then scrapped off and lysed with 3 volumes of 1X NP-40 buffer (50 mM HEPES-KOH pH7.5, 150 mM KCl, 2 mM EDTA, 0.5% NP-40, 10 mM β-ME, protease inhibitors and 400 U/ml RNase inhibitor). Clear cell lysates were treated with RNase T1 (Thermo Scientific) to a final concentration of 0.1 U/μl at room temperature for 15 minutes and immunoprecipitated with anti-Flag magnetic beads (M2; Sigma) at 4°C for 1 hour. Beads were washed three times with IP-wash buffer (50 mM HEPES-KOH pH7.5, 300 mM KCl, 0.05% NP-40. 10 mM β-ME, protease inhibitors and 200 U/ml RNase inhibitor) and treated with RNase T1 to a final concentration of 10 U/μl at room temperature for 15 minutes. SUPERase•In™ RNase Inhibitor (ThermoFisher) was then added to a final concentration of 1 U/μl to inhibit RNase T1. Beads were further washed three times with high-salt wash buffer (50 mM HEPES-KOH pH7.5, 500 mM KCl, 0.05% NP-40. 10 mM β-ME, protease inhibitors and 200 U/ml RNase inhibitor) and twice with PNK buffer (50 mM Tris-HCl pH7.5, 50 mM NaCl, 50 mM $MgCl_2$). Beads were treated with 10 μl of T4 Polynucleotide kinase (PNK; NEB) in 100 μl of 1X T4 PNK Reaction buffer containing 1 U/μl SUPERase•In™ RNase Inhibitor at 37°C for 30 minutes, followed by addition of 1 mM ATP and 5 μl PNK for another 30 minutes incubation. After removal of the supernatants, beads were incubated with proteinase K at 55°C for 30 minutes with shaking. The supernatants were collected and RNAs were

purified by using RNA Clean & Concentrator-5 kit (Zymo Research). The purified RNAs were subjected to library preparation by using NEB Next® Small RNA Library Prep Set for Illumina® (NEB #7300) and sequenced by Illumina HiSeq.

The single-end CLIP-Seq raw data was trimmed with flexbar (version 3.5.0, https://github.com/seqan/flexbar) tool to remove adapters and low-quality reads (length shorter than 20). Remaining reads were aligned to the human genome (GENCODE v37 GRCh38, https://www.gencodegenes.org) using STAR (version 2.7.8a, https://github.com/alexdobin/STAR). The rRNA and PCR duplicated reads were removed using bedtools (version 2.30.0, https://bedtools.readthedocs.io) and samtools (version 1.12, http://www.htslib.org), respectively. The filtered BAM files were used in the CLAM pipeline (version 1.2.0, https://github.com/Xinglab/CLAM) to define candidate cross-linking regions. The cross-linking signatures were detected from the RNF113A CLIP-Seq data (plus MMS treatment) using the empty vector CLIP-Seq data as control with set region bin as 100. To reduce false positives, the CLIP candidate cross-linking regions shared by all three replicates were used for downstream analysis. For the detected signals, Homer (version 4.11, http://homer.ucsd.edu/homer/ngs/annotation.html) was used to annotate the regions with specific genomic features.

Immunofluorescence microscopy—All immunofluorescence microscopy for foci analysis was performed as previously described (Brickner et al., 2017), with minor modifications. U2OS cells expressing NLS-tagged METTL8 or TRMT61A fusions were washed with 1× PBS prior to fixation with 3.2% paraformaldehyde. For YFP-MS2 analysis, the U2OS 2–6-3 expressing degron-tagged LacI fusion proteins were incubated with 300 nM Shield1 ligand (Takara Bio) and 1 μg/ml doxycycline for 24 hours, then washed with 1× PBS prior to fixation as above. For ASCC localization, U2OS 2–6-5 cells were treated as the 2–6-3 cells but were extracted with 1× PBS containing 0.2% Triton X-100 and protease inhibitor cocktail (Pierce) for 10–20 minutes on ice prior to fixation. For MMS-induced foci analysis, U2OS cells were treated with 500 μM MMS in complete medium at 37°C for six hours, washed with 1× PBS, then extracted and fixed as above. All cells were then washed extensively with IF Wash Buffer (1× PBS, 0.5% NP-40, and 0.02% NaN_3), then blocked with IF Blocking Buffer (IF Wash Buffer plus 10% FBS) for at least 30 minutes. Primary antibodies were diluted in IF Blocking Buffer overnight at 4°C. After staining with secondary antibodies (conjugated with Alexa Fluor 488 or 594; Millipore) and Hoechst 33342 (BD Bioscience), where indicated, samples were mounted using Prolong Gold mounting medium (Invitrogen). Epifluorescence microscopy was performed on an Olympus fluorescence microscope (BX-53) using an ApoN 60X/1.49 NA oil immersion lens or an UPlanS-Apo 100X/1.4 oil immersion lens and cellSens Dimension software. Raw images were exported into Adobe Photoshop, and for any adjustments in image contrast or brightness, the levels function was applied. For foci quantitation, at least 100 cells were analyzed in triplicate, unless otherwise indicated.

RNA-DNA hybrid (R-loop) quantification by immunofluorescence—Detection of s9.6 signal was performed as described previously (Wood et al., 2020). U2OS or HeLa cells were seeded on glass coverslips 24 hours before treatment. After treatment with MMS, coverslips were fixed with 100% ice-cold methanol for 10 min at −20 °C. Fixed coverslips

were treated with 6 μg/ml RNase A (Invitrogen) in RNase A buffer (10 mM Tris-HCl, 5 mM NaCl, 5 mM EDTA) for 30 min at 37°C to avoid non-specific binding of single-stranded RNA outside R-loops. Negative controls were created by additional incubation of slides with 6 μg/mL RNase H (NEB), for 2 hours at 37°C. Cells were then washed in PBS and then blocked in 5% BSA diluted in PBS for 30 min at 37°C followed by incubation with the s9.6 primary antibody (1:500; Kerafast) and rabbit anti-nucleolin primary antibody (1:2000; Abcam) for 1 hour in a humid chamber at 37°C. Secondary antibodies anti-mouse Alexa Fluor 546 and anti-rabbit Alexa Fluor 488 (both 1:1000; Thermo Fisher Scientific) and DAPI were incubated with cells for 30 minutes in a humidity chamber at 37°C. Coverslips were mounted onto glass slides using ProLong Gold (Invitrogen). Images were taken using a 63X objective with a confocal fluorescent microscope (LEICA: DMi8 TCS SPE). Only nuclear staining was used to quantify R-loop accumulation, and all cytoplasmic and nucleoli staining was removed before analysis. We subtracted cytoplasmic and nucleolar staining, as determined by co-staining with nucleolin. Images were analyzed using an ImageJ macro that sequentially subtracted nucleolin staining, detected and outlined nuclei based on DAPI staining, and measured mean integrated density of s9.6 staining in nuclei to avoid bias. At least 100 cells were counted for each individual replicate.

His-ubiquitin pulldown assays—His-tagged ubiquitin was immunoprecipitated after denaturation as described previously (Gajjar et al., 2012; Xirodimas et al., 2001), with minor modifications. Briefly, HeLa cells expressing Flag-HA-RNF113A WT, Flag-HA-RNF113A I264A or Flag-HA-RNF113A ΔRING were transfected with His-Ub. At ~42 hours after transfection, cells were exposed MMS (500 μM). The cells were harvested, washed twice with cold 1x PBS and lysed in 1 ml of Lysis buffer (6 M guanidinium-HCl, 100 mM Na_2HPO_4/NaH_2PO_4, 10 mM Tris-HCl pH 8.0, 5 mM imidazole, 10 mM β-mercaptoethanol, and protease inhibitors). Cells were sonicated on ice for 10 seconds twice and centrifuged at 11K rpm at 4°C for 10 min. The supernatant was collected in a new tube and 4 ml of Lysis buffer was added. Ni-NTA-agarose beads were washed four times with Lysis buffer, added to the lysate and incubated for 4 hours at room temperature with rotation. Samples were washed for 5 min at room temperature once with Lysis buffer, once with Wash buffer (8 M urea, 100 mM Na_2HPO_4/NaH_2PO_4, 10 mM Tris-HCl pH 6.8, 5 mM imidazole, 10 mM β-mercaptoethanol, and protease inhibitors), and twice with Wash Buffer plus 0.1% Triton X-100. Beads were then incubated with Elution Buffer (50 mM Tris-HCl pH 7.3, 250 mM NaCl, 400 mM imidazole, 0.05% Triton X-100, 3 mM β-mercaptoethanol, and protease inhibitors) overnight at 4°C. After elution, 4x Laemmli Buffer was added, and samples were analyzed by Western Blotting.

Tandem ubiquitin binding element (TUBE) assays—HeLa-S cells (~$6–8 \times 10^7$) grown in a spinner flask were treated with the indicated genotoxic agents (1 mM MMS, 10 mM hydroxyurea, 20 μM bleomycin, 1 μM camptothecin, 200 μM H_2O_2, or otherwise indicated) for four hours at 37°C. The cells were collected by centrifugation, and washed with ice-cold PBS and frozen at −80°C as two cell pellets. Each cell pellet was resuspended in 10 ml TUBE lysis buffer (50 mM Tris·HCl, pH 7.5, 1 mM EGTA, 1 mM EDTA, 1% (v/v) Triton X-100, and 0.27 M sucrose) containing freshly added 100 mM iodoacetamide, protease and phosphatase inhibitors, then rotated at 4°C for one hour for lysis. The extract

was spun at 6500 rpm for 30 minutes. Supernatant was transferred to a fresh tube and spun at 6500 rpm for 5 minutes. A fraction of the spun extract was kept as input, and the rest was rotated overnight at 4°C with 50 μl commercial ubiquilin-conjugated TUBE beads (Boston Biochem) or HALO-conjugated TUBE beads (Zhao et al., 2018). The beads were washed three times with 10 ml high salt TAP buffer (50 mM Tris-HCl, pH 7.9, 300 mM KCl, 5 mM $MgCl_2$, 0.2 mM EDTA, 0.1% NP-0, 10% glycerol, 2 mM β-mercaptoethanol, 0.2 mM PMSF) and once with 1 ml low salt TAP buffer (50 mM Tris-HCl, pH 7.9, 0 mM KCl, 5 mM $MgCl_2$, 0.2 mM EDTA, 0.1% NP-0, 10% glycerol, 2 mM β-mercaptoethanol, 0.2 mM PMSF). Beads were resuspended in 50 μl Laemmli buffer and analyzed by Western blotting.

Ubiquitin ligase assays—Reactions analyzing ubiquitin chain polymerization were performed in ubiquitin ligase buffer (25 mM Tris pH 7.3, 25 mM NaCl, 10 mM $MgCl_2$, 100 nM $ZnCl_2$, 1 mM β-mercaptoethanol) containing 2 mM ATP and 10 μM of ubiquitin in a total volume of 20 μl. E1 activating enzyme (UBE1; Boston Biochem) was used at 31.25 nM, and E2 ubiquitin conjugating enzymes (Ubch5c; Boston Biochem) were used at 0.625 μM. Flag-tagged-RNF113A purified from HeLa-S cells with or without treatment with MMS was added to each reaction and incubated at 37°C for 3 hours. For the reactions incubated with nucleic acid, Flag-tagged-RNF113A or RNF113A mutant proteins purified from HeLa-S cells was used at 0.1 μM. *In vitro*-transcribed β-globin pre-mRNA with or without treatment with DMS, as well as DNA or RNA oligonucleotides with or without single m1A in the sequences were added as indicated concentrations and incubated at 37°C for 1.5 hours. Reactions were stopped with 20 μl of Laemmli buffer, analyzed by SDS-PAGE, and Western blotted.

QUANTIFICATION AND STATISTICAL ANALYSIS

Where relevant, data is represented as the mean of the indicated number of replicates and error bars represent the standard deviation of the mean. All *p*-values, except where indicated, were calculated by Student's *t*-test. RNA-Seq box plot *p*-values were determined by an exact permutation of the Wilcoxon-Mann-Whitney as described (Marx et al., 2016). R-loop analysis *p*-values were determined by repeated measure one-way ANOVA with Tukey's multiple comparisons test, with a single pooled variance.

Supplementary Material

Refer to Web version on PubMed Central for supplementary material.

Acknowledgments

We wish to thank Yang Shi, Hani Zaher, and the Structural Cell Biology of DNA Repair Machines (SBDR) members for their advice on this manuscript. We acknowledge the Extreme Science and Engineering Discovery Environment (XSEDE, PSC allocations TG-BIO160040 and TG-MCB170053), which is supported by NSF grant ACI-1548562. J.A.T. acknowledges support as a CPRIT Scholar in Cancer Research and Robert A. Welch Distinguished Chair in Chemistry. This work was supported by the ANR (ANR-16-CE11-0018 to N.R.), the INCa (PLBIO19-021 to N.R.), the NIH SBDR program project (P01 CA092584, to J.A.T. and N.M.), R01 CA237263 and R01 CA248526 (to A.V.), R01 CA193318 and R01 CA227001 (to N.M.), the DOD BRCP Expansion Award (BC191374 to A.V.), an American Cancer Society Research Scholar Award (RSG-18-156-01-DMC to N.M.), the Barnard Foundation (to N.M.) and by the Alvin J. Siteman Cancer Center Siteman Investment Program (supported by The Foundation for Barnes-Jewish Hospital, Cancer Frontier Fund, to A.V. and N.M.). C.H. is an investigator of the Howard Hughes Medical Institute.

References

Aas PA, Otterlei M, Falnes PO, Vagbo CB, Skorpen F, Akbari M, Sundheim O, Bjoras M, Slupphaug G, Seeberg E, et al. (2003). Human and bacterial oxidative demethylases repair alkylation damage in both RNA and DNA. Nature 421, 859–863. [PubMed: 12594517]

Bader AS, Hawley BR, Wilczynska A, and Bushell M. (2020). The roles of RNA in DNA double-strand break repair. Br J Cancer 122, 613–623. [PubMed: 31894141]

Brickner JR, Soll JM, Lombardi PM, Vagbo CB, Mudge MC, Oyeniran C, Rabe R, Jackson J, Sullender ME, Blazosky E, et al. (2017). A ubiquitin-dependent signalling axis specific for ALKBH-mediated DNA dealkylation repair. Nature 551, 389–393. [PubMed: 29144457]

Brickner JR, Townley BA, and Mosammaparast N. (2019). Intersections between transcription-coupled repair and alkylation damage reversal. DNA Repair (Amst) 81, 102663. [PubMed: 31326362]

Butler M, Pongor L, Su YT, Xi L, Raffeld M, Quezado M, Trepel J, Aldape K, Pommier Y, and Wu J. (2020). MGMT Status as a Clinical Biomarker in Glioblastoma. Trends Cancer 6, 380–391. [PubMed: 32348734]

Byrum AK, Carvajal-Maldonado D, Mudge MC, Valle-Garcia D, Majid MC, Patel R, Sowa ME, Gygi SP, Harper JW, Shi Y, et al. (2019). Mitotic regulators TPX2 and Aurora A protect DNA forks during replication stress by counteracting 53BP1 function. The Journal of cell biology 218, 422–432. [PubMed: 30602538]

Cretu C, Agrawal AA, Cook A, Will CL, Fekkes P, Smith PG, Luhrmann R, Larsen N, Buonamici S, and Pena V. (2018). Structural Basis of Splicing Modulation by Antitumor Macrolide Compounds. Mol Cell 70, 265–273 e268. [PubMed: 29656923]

D'Silva S, Haider SJ, and Phizicky EM (2011). A domain of the actin binding protein Abp140 is the yeast methyltransferase responsible for 3-methylcytidine modification in the tRNA anti-codon loop. Rna 17, 1100–1110. [PubMed: 21518804]

Dango S, Mosammaparast N, Sowa ME, Xiong LJ, Wu F, Park K, Rubin M, Gygi S, Harper JW, and Shi Y. (2011). DNA unwinding by ASCC3 helicase is coupled to ALKBH3-dependent DNA alkylation repair and cancer cell proliferation. Mol Cell 44, 373–384. [PubMed: 22055184]

Dobin A, Davis CA, Schlesinger F, Drenkow J, Zaleski C, Jha S, Batut P, Chaisson M, and Gingeras TR (2013). STAR: ultrafast universal RNA-seq aligner. Bioinformatics 29, 15–21. [PubMed: 23104886]

Drablos F, Feyzi E, Aas PA, Vaagbo CB, Kavli B, Bratlie MS, Pena-Diaz J, Otterlei M, Slupphaug G, and Krokan HE (2004). Alkylation damage in DNA and RNA--repair mechanisms and medical significance. DNA Repair (Amst) 3, 1389–1407. [PubMed: 15380096]

Eng JK, McCormack AL, and Yates JR (1994). An approach to correlate tandem mass spectral data of peptides with amino acid sequences in a protein database. J Am Soc Mass Spectrom 5, 976–989. [PubMed: 24226387]

Fedeles BI, Singh V, Delaney JC, Li D, and Essigmann JM (2015). The AlkB Family of Fe(II)/alpha-Ketoglutarate-dependent Dioxygenases: Repairing Nucleic Acid Alkylation Damage and Beyond. J Biol Chem 290, 20734–20742. [PubMed: 26152727]

Fu D, Calvo JA, and Samson LD (2012). Balancing repair and tolerance of DNA damage caused by alkylating agents. Nat Rev Cancer 12, 104–120. [PubMed: 22237395]

Gajjar M, Candeias MM, Malbert-Colas L, Mazars A, Fujita J, Olivares-Illana V, and Fahraeus R. (2012). The p53 mRNA-Mdm2 interaction controls Mdm2 nuclear trafficking and is required for p53 activation following DNA damage. Cancer Cell 21, 25–35. [PubMed: 22264786]

Haselbach D, Komarov I, Agafonov DE, Hartmuth K, Graf B, Dybkov O, Urlaub H, Kastner B, Luhrmann R, and Stark H. (2018). Structure and Conformational Dynamics of the Human Spliceosomal B(act) Complex. Cell 172, 454–464 e411. [PubMed: 29361316]

Janicki SM, Tsukamoto T, Salghetti SE, Tansey WP, Sachidanandam R, Prasanth KV, Ried T, Shav-Tal Y, Bertrand E, Singer RH, et al. (2004). From silencing to gene expression: real-time analysis in single cells. Cell 116, 683–698. [PubMed: 15006351]

Juszkiewicz S, Speldewinde SH, Wan L, Svejstrup JQ, and Hegde RS (2020). The ASC-1 Complex Disassembles Collided Ribosomes. Mol Cell.

Li X, Xiong X, Zhang M, Wang K, Chen Y, Zhou J, Mao Y, Lv J, Yi D, Chen XW, et al. (2017). Base-Resolution Mapping Reveals Distinct m(1)A Methylome in Nuclear- and Mitochondrial-Encoded Transcripts. Mol Cell 68, 993–1005 e1009. [PubMed: 29107537]

Liao Y, Smyth GK, and Shi W. (2014). featureCounts: an efficient general purpose program for assigning sequence reads to genomic features. Bioinformatics 30, 923–930. [PubMed: 24227677]

Liu F, Clark W, Luo G, Wang X, Fu Y, Wei J, Wang X, Hao Z, Dai Q, Zheng G, et al. (2016). ALKBH1-Mediated tRNA Demethylation Regulates Translation. Cell 167, 1897.

Liu R, Holik AZ, Su S, Jansz N, Chen K, Leong HS, Blewitt ME, Asselin-Labat ML, Smyth GK, and Ritchie ME (2015). Why weight? Modelling sample and observational level variability improves power in RNA-seq analyses. Nucleic Acids Res 43, e97. [PubMed: 25925576]

Luo W, Friedman MS, Shedden K, Hankenson KD, and Woolf PJ (2009). GAGE: generally applicable gene set enrichment for pathway analysis. BMC Bioinformatics 10, 161. [PubMed: 19473525]

Marx A, Backes C, Meese E, Lenhof HP, and Keller A. (2016). EDISON-WMW: Exact Dynamic Programing Solution of the Wilcoxon-Mann-Whitney Test. Genomics Proteomics Bioinformatics 14, 55–61. [PubMed: 26829645]

Matsuo Y, Tesina P, Nakajima S, Mizuno M, Endo A, Buschauer R, Cheng J, Shounai O, Ikeuchi K, Saeki Y, et al. (2020). RQT complex dissociates ribosomes collided on endogenous RQC substrate SDD1. Nat Struct Mol Biol 27, 323–332. [PubMed: 32203490]

Mazina OM, Keskin H, Hanamshet K, Storici F, and Mazin AV (2017). Rad52 Inverse Strand Exchange Drives RNA-Templated DNA Double-Strand Break Repair. Mol Cell 67, 19–29 e13. [PubMed: 28602639]

Movassat M, Mueller WF, and Hertel KJ (2014). In vitro assay of pre-mRNA splicing in mammalian nuclear extract. Methods in molecular biology 1126, 151–160. [PubMed: 24549662]

Noma A, Yi S, Katoh T, Takai Y, Suzuki T, and Suzuki T. (2011). Actin-binding protein ABP140 is a methyltransferase for 3-methylcytidine at position 32 of tRNAs in Saccharomyces cerevisiae. Rna 17, 1111–1119. [PubMed: 21518805]

Ougland R, Zhang CM, Liiv A, Johansen RF, Seeberg E, Hou YM, Remme J, and Falnes PO (2004). AlkB restores the biological function of mRNA and tRNA inactivated by chemical methylation. Mol Cell 16, 107–116. [PubMed: 15469826]

Patro R, Duggal G, Love MI, Irizarry RA, and Kingsford C. (2017). Salmon provides fast and bias-aware quantification of transcript expression. Nat Methods 14, 417–419. [PubMed: 28263959]

Ritchie ME, Phipson B, Wu D, Hu Y, Law CW, Shi W, and Smyth GK (2015). limma powers differential expression analyses for RNA-sequencing and microarray studies. Nucleic Acids Res 43, e47. [PubMed: 25605792]

Robinson MD, McCarthy DJ, and Smyth GK (2010). edgeR: a Bioconductor package for differential expression analysis of digital gene expression data. Bioinformatics 26, 139–140. [PubMed: 19910308]

Safra M, Sas-Chen A, Nir R, Winkler R, Nachshon A, Bar-Yaacov D, Erlacher M, Rossmanith W, Stern-Ginossar N, and Schwartz S. (2017). The m1A landscape on cytosolic and mitochondrial mRNA at single-base resolution. Nature 551, 251–255. [PubMed: 29072297]

Sakaue-Sawano A, Kurokawa H, Morimura T, Hanyu A, Hama H, Osawa H, Kashiwagi S, Fukami K, Miyata T, Miyoshi H, et al. (2008). Visualizing spatiotemporal dynamics of multicellular cell-cycle progression. Cell 132, 487–498. [PubMed: 18267078]

Schwertman P, Bekker-Jensen S, and Mailand N. (2016). Regulation of DNA double-strand break repair by ubiquitin and ubiquitin-like modifiers. Nat Rev Mol Cell Biol 17, 379–394. [PubMed: 27211488]

Shanbhag NM, Rafalska-Metcalf IU, Balane-Bolivar C, Janicki SM, and Greenberg RA (2010). ATM-dependent chromatin changes silence transcription in cis to DNA double-strand breaks. Cell 141, 970–981. [PubMed: 20550933]

Soll JM, Sobol RW, and Mosammaparast N. (2017). Regulation of DNA Alkylation Damage Repair: Lessons and Therapeutic Opportunities. Trends in biochemical sciences 42, 206–218. [PubMed: 27816326]

Song L, and Luo ZQ (2019). Post-translational regulation of ubiquitin signaling. The Journal of cell biology 218, 1776–1786. [PubMed: 31000580]

Sundheim O, Vagbo CB, Bjoras M, Sousa MM, Talstad V, Aas PA, Drablos F, Krokan HE, Tainer JA, and Slupphaug G. (2006). Human ABH3 structure and key residues for oxidative demethylation to reverse DNA/RNA damage. EMBO J25, 3389–3397. [PubMed: 16858410]

Tijerina P, Mohr S, and Russell R. (2007). DMS footprinting of structured RNAs and RNA-protein complexes. Nat Protoc 2, 2608–2623. [PubMed: 17948004]

Ueda Y, Ooshio I, Fusamae Y, Kitae K, Kawaguchi M, Jingushi K, Hase H, Harada K, Hirata K, and Tsujikawa K. (2017). AlkB homolog 3-mediated tRNA demethylation promotes protein synthesis in cancer cells. Scientific reports 7, 42271. [PubMed: 28205560]

Vagbo CB, Svaasand EK, Aas PA, and Krokan HE (2013). Methylation damage to RNA induced in vivo in Escherichia coli is repaired by endogenous AlkB as part of the adaptive response. DNA Repair (Amst) 12, 188–195. [PubMed: 23276627]

van den Born E, Omelchenko MV, Bekkelund A, Leihne V, Koonin EV, Dolja VV, and Falnes PO (2008). Viral AlkB proteins repair RNA damage by oxidative demethylation. Nucleic Acids Res 36, 5451–5461. [PubMed: 18718927]

van den Born E, Vagbo CB, Songe-Moller L, Leihne V, Lien GF, Leszczynska G, Malkiewicz A, Krokan HE, Kirpekar F, Klungland A, et al. (2011). ALKBH8-mediated formation of a novel diastereomeric pair of wobble nucleosides in mammalian tRNA. Nat Commun 2, 172. [PubMed: 21285950]

Wang L, Wang S, and Li W. (2012). RSeQC: quality control of RNA-seq experiments. Bioinformatics 28, 2184–2185. [PubMed: 22743226]

Wang X, Lu Z, Gomez A, Hon GC, Yue Y, Han D, Fu Y, Parisien M, Dai Q, Jia G, et al. (2014). N6-methyladenosine-dependent regulation of messenger RNA stability. Nature 505, 117–120. [PubMed: 24284625]

Williamson L, Saponaro M, Boeing S, East P, Mitter R, Kantidakis T, Kelly GP, Lobley A, Walker J, Spencer-Dene B, et al. (2017). UV Irradiation Induces a Non-coding RNA that Functionally Opposes the Protein Encoded by the Same Gene. Cell 168, 843–855 e813. [PubMed: 28215706]

Wood M, Quinet A, Lin YL, Davis AA, Pasero P, Ayala YM, and Vindigni A. (2020). TDP-43 dysfunction results in R-loop accumulation and DNA replication defects. J Cell Sci 133.

Xirodimas D, Saville MK, Edling C, Lane DP, and Lain S. (2001). Different effects of p14ARF on the levels of ubiquitinated p53 and Mdm2 in vivo. Oncogene 20, 4972–4983. [PubMed: 11526482]

Xu L, Liu X, Sheng N, Oo KS, Liang J, Chionh YH, Xu J, Ye F, Gao YG, Dedon PC, et al. (2017). Three distinct 3-methylcytidine (m(3)C) methyltransferases modify tRNA and mRNA in mice and humans. J Biol Chem 292, 14695–14703. [PubMed: 28655767]

Yan C, Wan R, Bai R, Huang G, and Shi Y. (2016). Structure of a yeast activated spliceosome at 3.5 A resolution. Science 353, 904–911. [PubMed: 27445306]

Yan LL, Simms CL, McLoughlin F, Vierstra RD, and Zaher HS (2019). Oxidation and alkylation stresses activate ribosome-quality control. Nat Commun 10, 5611. [PubMed: 31819057]

Zhang LS, Liu C, Ma H, Dai Q, Sun HL, Luo G, Zhang Z, Zhang L, Hu L, Dong X, et al. (2019). Transcriptome-wide Mapping of Internal N(7)-Methylguanosine Methylome in Mammalian mRNA. Mol Cell 74, 1304–1316 e1308. [PubMed: 31031084]

Zhao Y, Mudge MC, Soll JM, Rodrigues RB, Byrum AK, Schwarzkopf EA, Bradstreet TR, Gygi SP, Edelson BT, and Mosammaparast N. (2018). OTUD4 Is a Phospho-Activated K63 Deubiquitinase that Regulates MyD88-Dependent Signaling. Mol Cell 69, 505–516 e505. [PubMed: 29395066]

Highlights

- Alkylated RNA, but not DNA, recruits ASCC-ALKBH3 in an RNF113A-dependent manner
- This alkylation repair pathway suppresses transcription and R-loop accumulation
- Alkylated pre-mRNA activates RNF113A E3 ligase activity *in vitro*

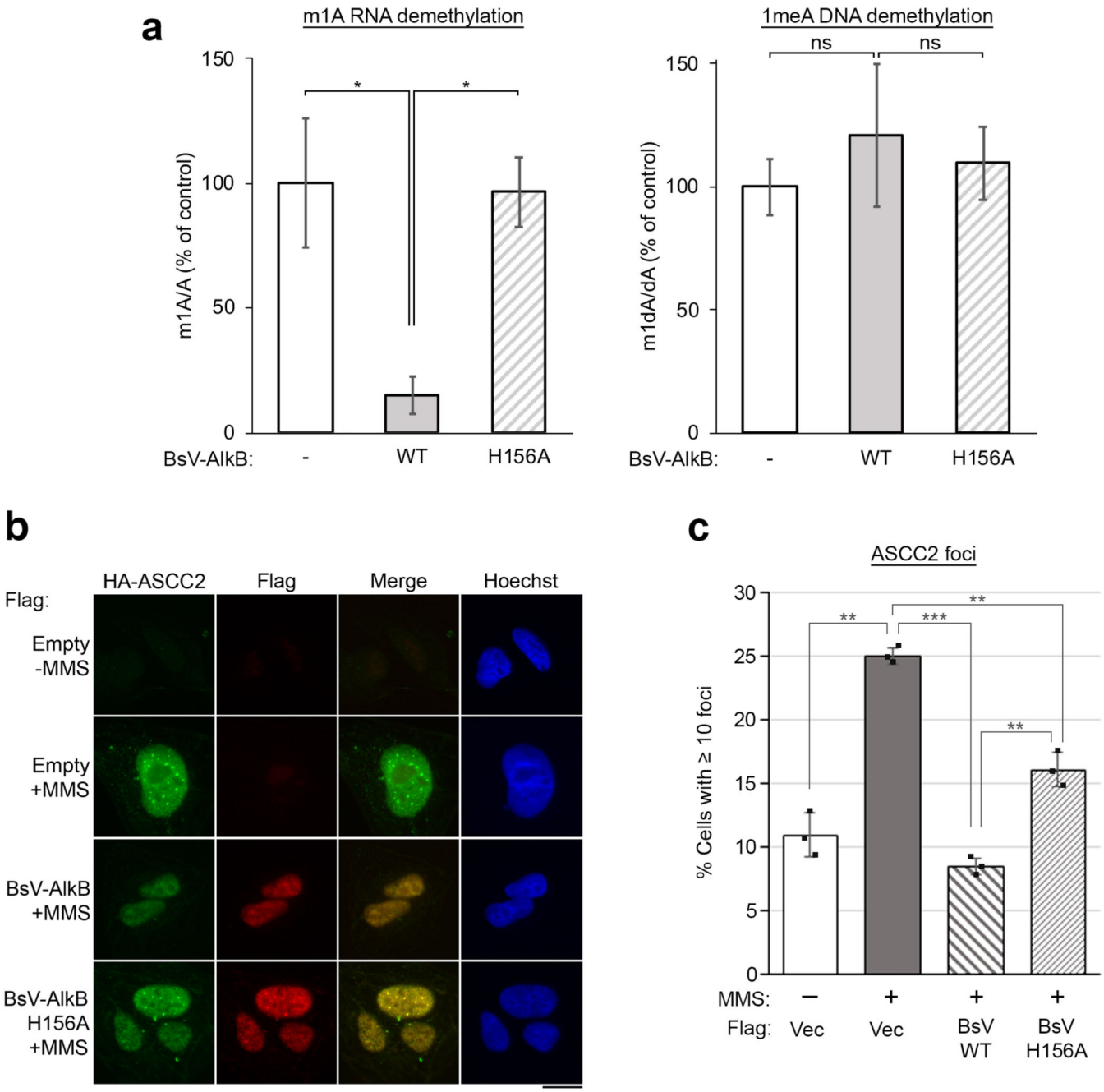

Figure 1. RNA alkylation is necessary for ASCC recruitment to nuclear foci during.

(a) *In vitro* demethylation assays on identical sequences of m1A-containing RNA (left) or 1meA DNA oligonucleotide (right) with wildtype or catalytically inactive (H156A) BsV-AlkB protein. Reactions were quantified by LC-MS/MS and shown as a percent of no protein control (n=4 to 5 independent replicates; error bars indicate ± S.D. of the mean; * = $p < 0.05$).**(b)** U2OS cells expressing HA-ASCC2, as well as indicated Flag vectors were treated with MMS (500 μM) for six hours, then processed for immunofluorescence after Triton X-100 extraction. Scale bar, 10 μm. **(c)** Quantification of **(b)**. (n=3 biological replicates; error bars indicate ± S.D. of the mean; ** = $p < 0.001$, *** = $p < 0.0001$).

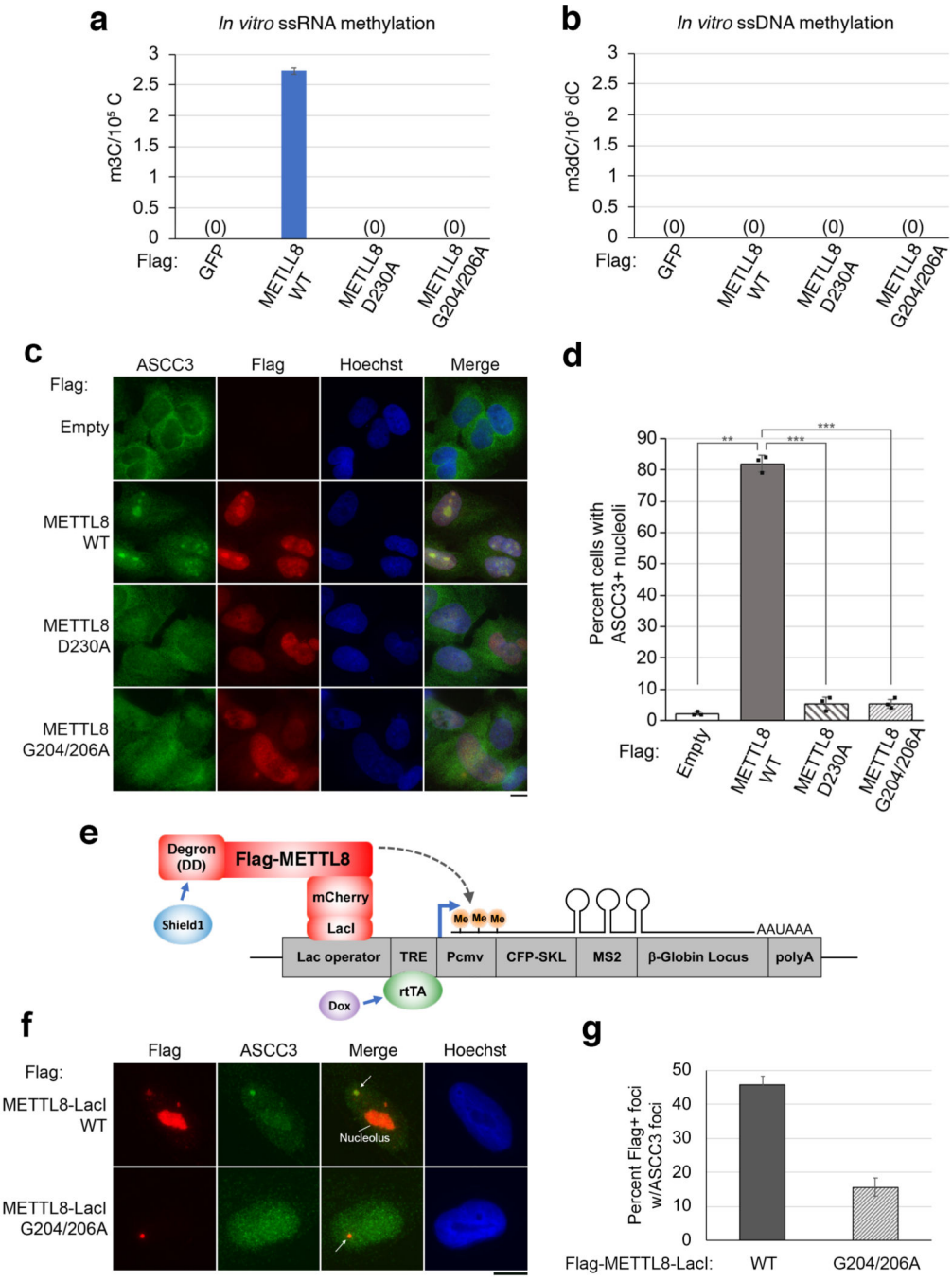

Figure 2. RNA alkylation is sufficient to recruit ASCC.

(a) and **(b)** *In vitro* methyltransferase assays were performed using Flag-tagged proteins with RNA **(a)** or DNA **(b)** oligonucleotides. Products were digested and quantified using LC-MS/MS. N = 2 independent replicates and error bars indicate ± S.D. of the mean. **(c)** U2OS cells expressing Flag vectors were processed for immunofluorescence using the indicated antibodies. Scale bar, 10 μm. **(d)** Quantification of **(c)** (n=3 replicates; error bars indicate ± S.D. of the mean; ** = $p < 0.001$, *** = $p < 0.0001$). **(e)** Locus reporter system to target METTL8 activity. **(f)** METTL8-catalyzed ASCC3 recruitment to the targeted locus.

The nucleolus and the reporter locus are shown. Scale bar, 10 μm. **(g)** Quantification of **(f)**. n=2 replicates; error bars indicate ± S.D. of the mean.

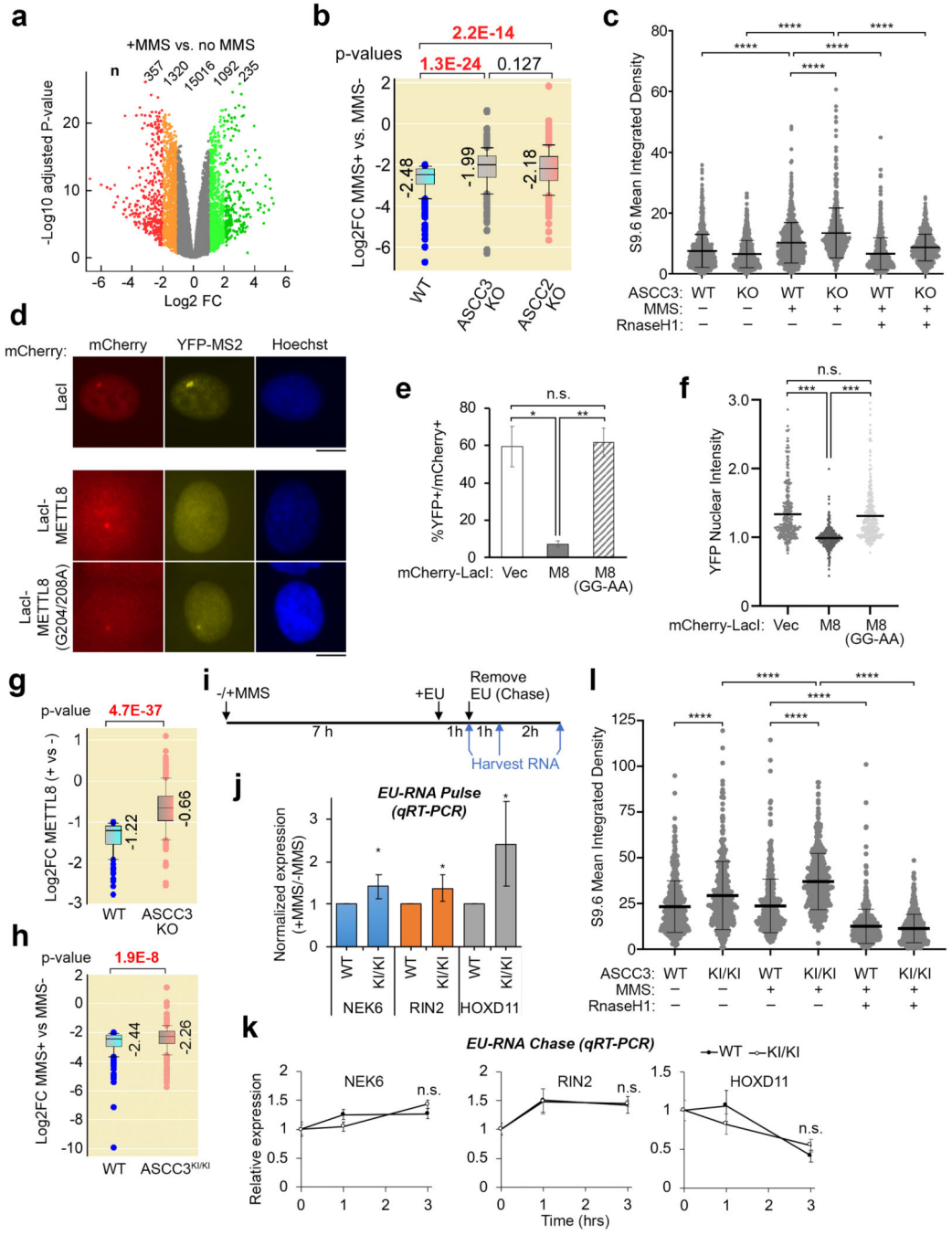

Figure 3. ASCC mediates transcriptional repression in response to aberrant RNA methylation.

(a) RNA-Seq analysis of WT U2OS cells ± MMS treatment (n=3 biological replicates). Genes upregulated or downregulated ±1 or ±2 $\log_2$ fold change (FC) with MMS are highlighted. **(b)** Box plot of downregulated genes upon MMS treatment (at least −2 $\log_2$ FC) in WT vs. ASCC3 and ASCC2 KO cells. **(c)** R-loop quantitation in WT and ASCC3 KO U2OS cells under the indicated conditions (n=4 independent replicates; error bars indicate ± S.D. of the mean; **** = p <0.0001 by one-way ANOVA with Tukey's multiple comparisons test, with single pooled variance). **(d)** METTL8-mediated nascent

gene repression as visualized by the MS2-YFP reporter system. The mCherry-LacI vector alone is shown separately due to different exposure time used solely for the mCherry-LacI control. Scale bar, 10 μm. **(e)** Quantification of MS2-YFP-positive/mCherry-positive foci from **(d)** (n=3 independent replicates; error bars indicate ± S.D. of the mean; * $p < 0.05$, ** $p < 0.01$, n.s. not significant). **(f)** Quantification of normalized YFP-MS2 nuclear foci intensities from **(d)** (n=3 independent replicates; error bars indicate ± S.D. of the mean; *** $p < 0.001$, n.s. not significant). **(g)** Box plot of downregulated genes upon DD-METTL8-NLS induction (at least −1 $\log_2$ FC) with Shield1 ligand in WT and ASCC3 KO cells. **(h)** Box plot of downregulated genes upon MMS treatment (at least −2 $\log_2$ FC) in WT and ASCC3$^{KI/KI}$ cells. **(i)** Scheme for nascent transcript analysis. Cells were treated with MMS, pulsed with EU, and EU was removed during a chase period. **(j)** Nascent transcript analysis of three genes from WT and ASCC3$^{KI/KI}$ cells after MMS treatment. N = 3 independent replicates; * $p < 0.05$. **(k)** Nascent transcript analysis of the same three genes from WT and ASCC3$^{KI/KI}$ cells after MMS treatment during the chase period. N = 3 independent replicates; n.s., not significant. **(l)** R-loop quantitation in WT and ASCC3$^{KI/KI}$ cells performed under the indicated conditions (n=3 independent replicates; error bars indicate ± S.D. of the mean; **** = $p < 0.0001$ by one-way ANOVA with Tukey's multiple comparisons test with single pooled variance).

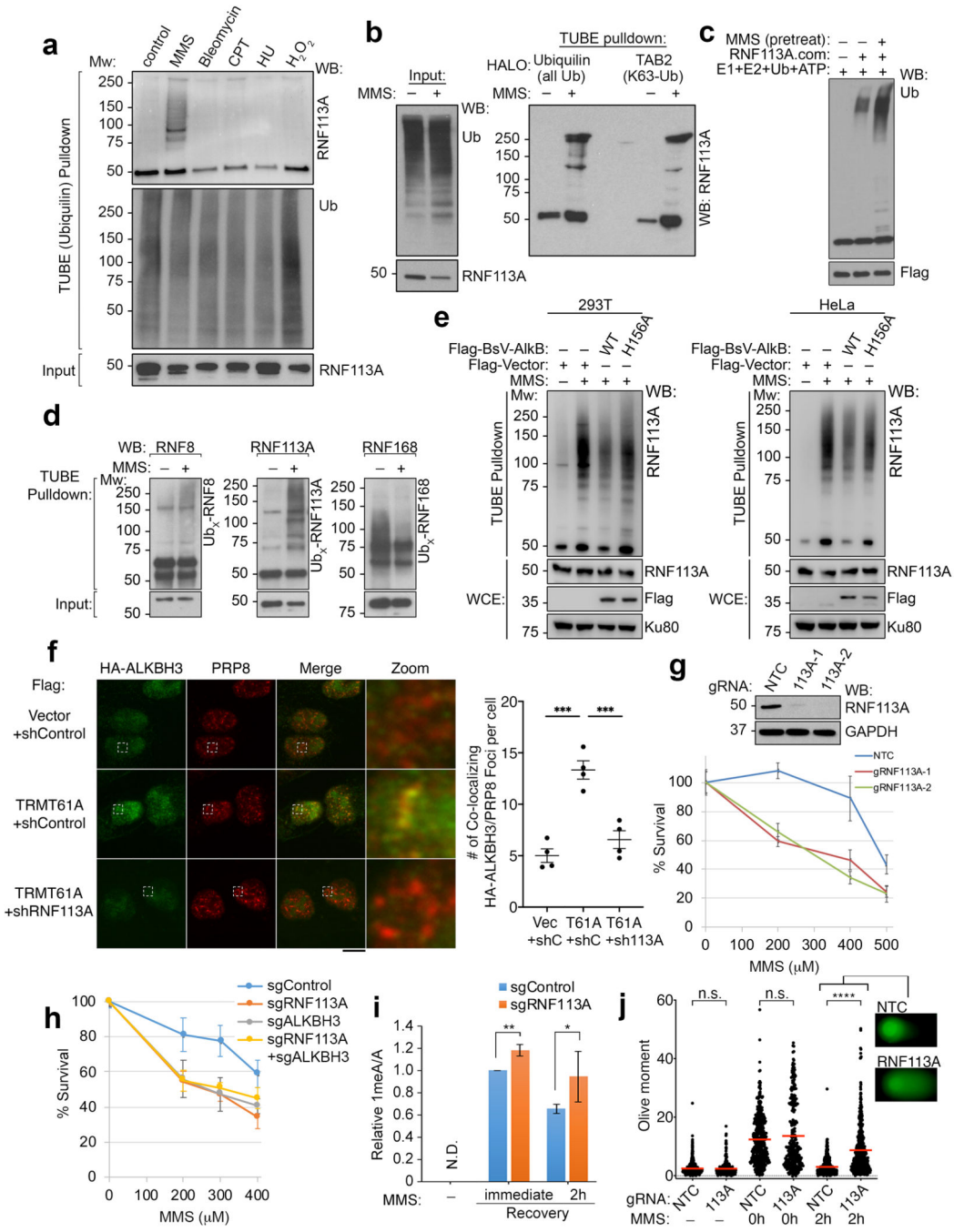

Figure 4. Alkylation damage selectively activates RNF113A E3 ligase.

(a) HeLa-S cells were treated with the indicated agents. Lysates were then used for tandem ubiquitin binding element (TUBE) pulldown using Ubiquilin-conjugated beads. Inputs and pulldown material were analyzed by Western blot (n=3 independent experiments). **(b)** TUBE pulldowns as in **(a)** using MMS, except that HALO-Ubiquilin (non-selective ubiquitin binding) or HALO-TAB2 (specific for K63 ubiquitin) beads were used. Input lysates are shown on the left. (n=3 independent experiments). **(c)** E3 ligase assays were performed using RNF113A purified from HeLa cells ± MMS pretreatment (n=3 independent

experiments). **(d)** TUBE pulldowns as in **(a)** using MMS, then probed for the different E3 ligases (n=2 independent experiments). **(e)** TUBE pulldowns as in **(a)** after transient (293T) or stable (HeLa) expression of the indicated vectors (n=2 independent experiments for each). **(f)** U2OS cells expressing HA-ALKBH3, Flag vector, and shRNA were used for immunofluorescence. Scale bar, 10 μm. A zoomed-in area is shown on the right. Quantification of co-localizing HA-ALKBH3/PRP8 foci is shown on the right. N = 4 replicates (combining two technical replicates of two independent experiments); *** $p <$ 0.001, error bars indicate ± S.D. of the mean. **(g)** Control or RNF113A-specific gRNAs were used for genome editing in HeLa cells. Resistance to MMS was determined by MTS assay (n=5 technical replicates for each). **(h)** The indicated KO cell lines were used to assess resistance to MMS using MTS assay (n=5 technical replicates). **(i)** Control or RNF113A-depleted cells were pulsed with 2.0 mM MMS for one hour, and incubated for another 0–2 hrs. Genomic DNA was isolated, digested, and assessed for 1meA/A using LC-MS/MS (n=4 biological replicates); ** $p < 0.01$. * $p < 0.05$. **(j)** Control or RNF113A-depleted cells were pulsed with 0.5 mM MMS for one hour, then incubated for the indicated periods of time. Neutral comet assay was used to assess DNA double-stranded breaks (N=3 independent replicates; error bars indicate ± S.D. of the mean; **** = $p <0.0001$ by one-way ANOVA with Tukey's multiple comparisons test with single pooled variance). Examples of comet tails are shown on the right.

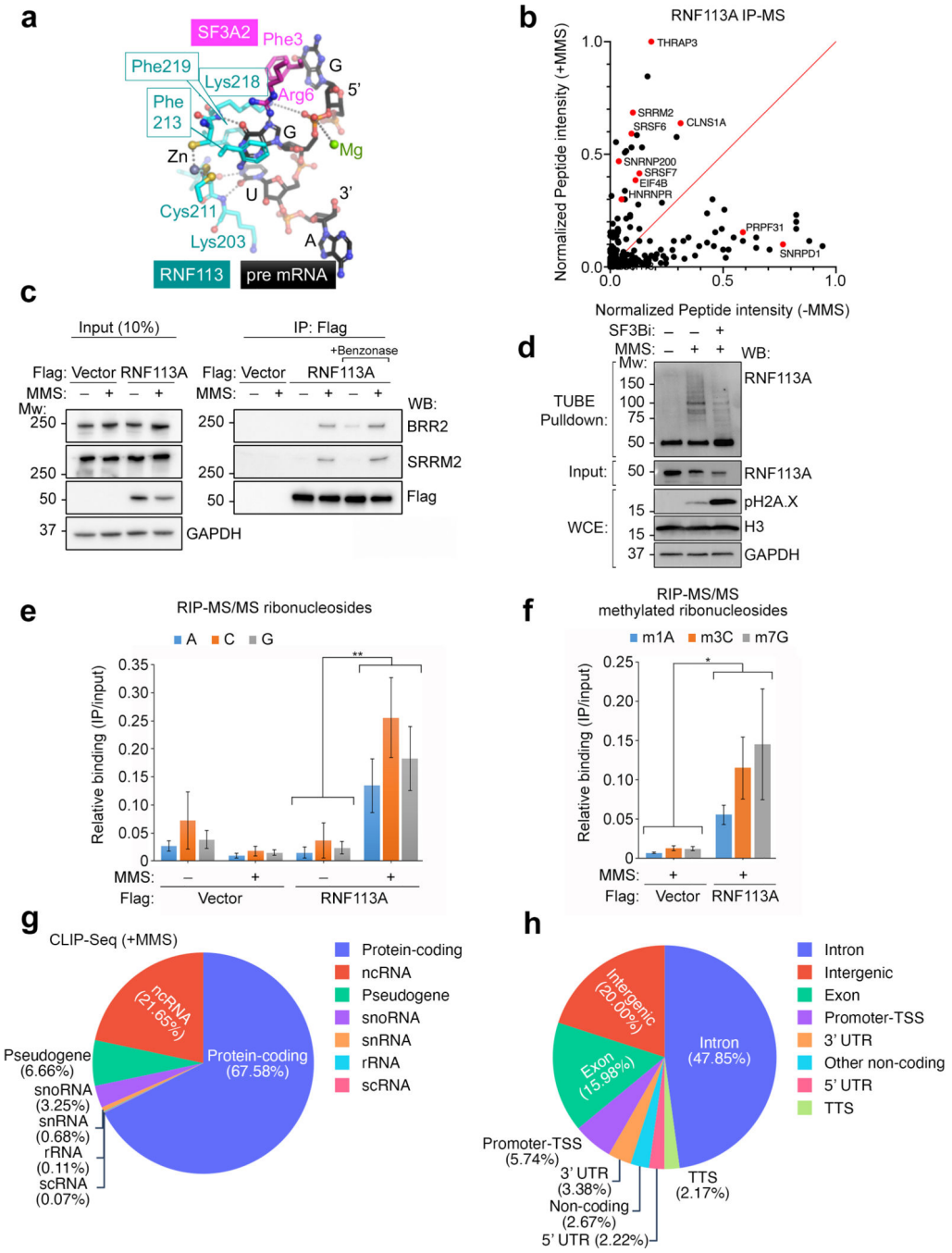

Figure 5. Characterization of RNF113A during alkylation damage.

(a) Stick representation of the 5´ splice site GU within the pre-mRNA and its interactions with RNF113A and SF3A2 (PDB: 6FF4). **(b)** Flag-tagged RNF113A was affinity purified from HeLa-S nuclear lysate with or without MMS treatment, then analyzed by LC-MS/MS. Total peptide intensities for the indicated proteins (normalized to RNF113A) were used to generate the scatter plot. **(c)** HeLa cells expressing the indicated Flag vector were used for immunoprecipitation with or without MMS treatment, in the presence or absence of benzonase. Bound and input material was analyzed as shown (n=3 independent

replicates). TUBE pulldowns were performed using HeLa-S cells treated with MMS and SF3B inhibitor as indicated, then probed by Western blot as shown (n=3 independent experiments). WCE indicates whole cell lysate. **(e)** and **(f)** HeLa-S cells expressing Flag-vector or Flag-RNF113A were subjected to RNA immunoprecipitation with or without prior MMS treatment. Purified RNAs were digested and the unmodified ribonucleosides **(e)** or methylated ribonucleosides **(f)** were analyzed by quantitative LC-MS/MS. The results are shown as the mean ± S.D. (n=3 independent replicates; * $p < 0.05$, ** $p < 0.01$). **(g)** and **(h)** CLIP-Seq analysis of RNF113A during MMS-induced damage. Categories of high confidence hits found in three biological replicates is shown in **(g)**, with specific regions mapped within protein coding RNAs shown in **(h)**.

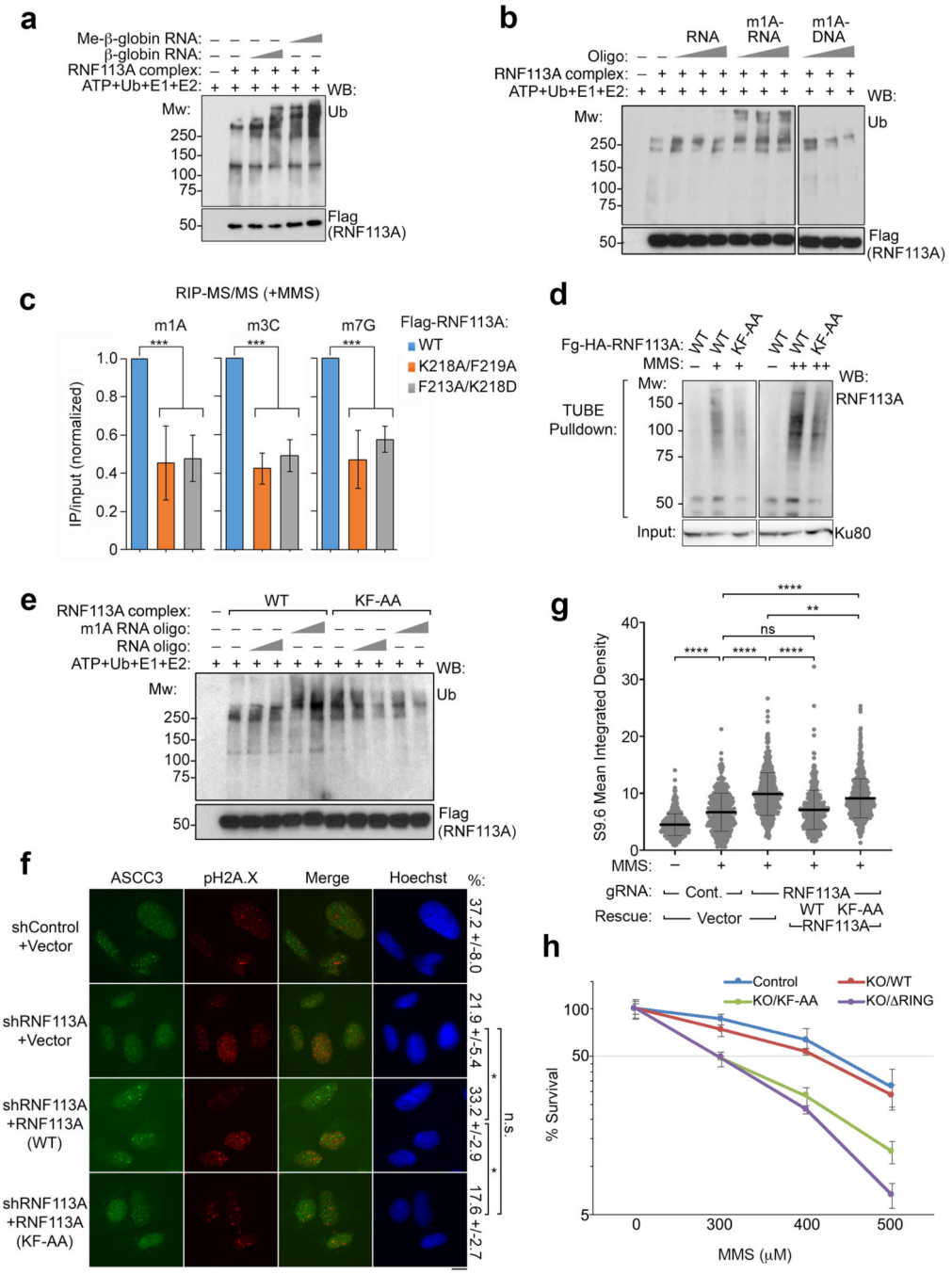

Figure 6. Alkylated RNA activates RNF113A *in vitro* and its ZnF domain is critical for its function in alkylation damage.

(a) RNF113A complex was immunopurified from untreated HeLa-S nuclear lysate, and *in vitro* E3 ligase assays were performed in the presence of the β-globin pre-mRNA (0.1 or 0.3 μM) with or without treatment with dimethyl sulfate as the methylating agent. The reaction products were analyzed by Western blotting using the antibodies as shown (n=3 independent experiments). **(b)** *In vitro* E3 ligase assays were performed as in **(a)** with the presence of 0.1, 0.2 or 0.5 μM single-stranded RNA, m1A-RNA or m1A-DNA oligonucleotides (n=2

independent experiments). Result with the m1A DNA (right) was from the same blot as the m1A RNA. **(c)** HeLa-S cells Flag-RNF113A wildtype (WT), Flag-RNF113A K218A/F219A, or Flag-RNF113A F123A/K218D were subjected to RNA immunoprecipitation (RIP). Purified RNAs were digested and the methylated nucleosides were analyzed by tandem mass spectrometry. The result was shown as the mean ± S.D. (n=3 independent replicates; * $p < 0.05$, ** $p < 0.01$). **(d)** TUBE assays were performed from HeLa cells expressing the Flag-HA tagged WT RNF113A or the K218A/F219A mutant, with or without two levels of MMS (100 or 250 μM) as shown. Ku80 was used as the input control. **(e)** *In vitro* E3 ligase assays were performed as in **(b)** with WT or K218A/F219A RNF113A complex in the reactions containing 0.1 or 0.3 μM RNA or m1A-RNA oligonucleotides (n=2 independent experiments). **(f)** U2OS cells expressing the indicated shRNAs were rescued with empty vector or the indicated RNF113A vectors. After MMS treatment, cells were processed for immunofluorescence staining using the indicated antibodies. Scale bar, 10 μm. Quantitation (defined as % cells having > 5 foci) is shown on the right for each condition, as the mean ± S.D. (n=3 independent replicates; * $p < 0.05$; n.s, not significant). **(g)** R-loop quantitation in HeLa cells expressing the indicated combinations of gRNA and rescue vectors was performed under the indicated conditions (n=4 replicates; error bars indicate ± S.D. of the mean; **** = $p < 0.0001$ and ** = $p < 0.01$ by repeated measure one-way ANOVA with Tukey's multiple comparisons test, with a single pooled variance). **(h)** HeLa cells were transduced with control gRNA or RNF113A-specific gRNAs, along with the indicated rescue vectors. Resistance to MMS was determined using MTS assay (n=5 technical replicates for each gRNA/rescue vector condition combination).

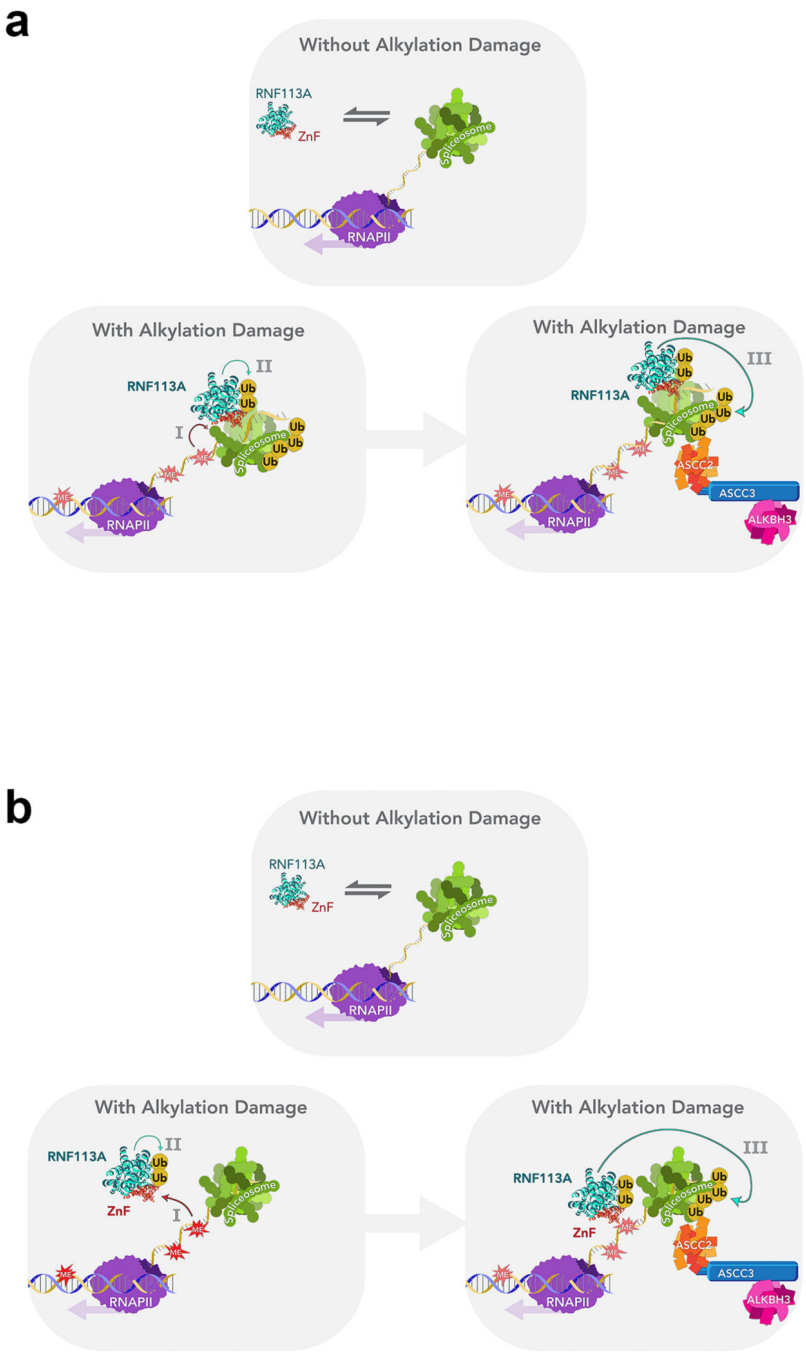

Figure 7. Models for the RNF113A-ASCC pathway.

In the preferred model **(a)**, RNF113A becomes stably associated with the spliceosome upon methylation damage to nascent RNA. activating the RNF113A E3 ligase, which in turn recruits the ASCC complex. **(b)** In the alternative model, the ZnF domain of RNF113A senses the aberrant methylation directly, while also associating with the spliceosome, activating its E3 ligase activity.

KEY RESOURCES TABLE

Reagent or Resource:	Source:	Identifier:
Antibodies		
6x-His (Mouse)	Abcam (ab18184)	ab18184
ASCC3 (Rabbit)	(Dango, *et. al.* 2011)	N/A
Flag (Mouse)	Sigma	F3165
Flag (Rabbit)	Sigma	F7425
GAPDH (Rabbit)	Abcam	ab181602
HA (Mouse)	BioLegend	901501
Nucleolin (Rabbit; for METTL8/TRMT61A staining)	Bethyl	A300-711A-T
Nucleolin (Rabbit; for S9.6 staining)	Abcam	ab22758
pH2A.X (Mouse)	Abcam	ab26350
pH2A.X (Rabbit)	Active Motif	39117
RNF113A (Rabbit)	Sigma	HPA000160
RNF8 (Rabbit)	Abcam	ab105362
RNF168 (Rabbit)	Gift of D. Durocher (U of Toronto)	N/A
Ubiquitin (Mouse)	Santa Cruz	sc-8017
β-actin HRP	Sigma	A3854
BRR2 (Rabbit)	Bethyl	A303–454A
SRRM2 (Rabbit)	Biorbyt	orb337685
S9.6	Kerafast	ENH001
Anti-rabbit Alexa Fluor 488	Thermo Fisher	A11034
Anti-mouse Alexa Fluor 546	Thermo Fisher	A21123
Anti-mouse Alexa Fluor 594	Thermo Fisher	A32742
Chemicals, peptides, recombinant proteins		
His-BsV-AlkB (bacterial)	This study	N/A
His-BsV-AlkB (H156A; bacterial)	This study	N/A
His-hALKBH3	This study	N/A
Flag-METTL8-NLS (HEK293T)	This study	N/A
Flag-METTL8-NLS (D230A; HEK239T)	This study	N/A
Flag-METTL8-NLS (G204A/G206A; HEK239T)	This study	N/A
Flag-RNF113A-WT (HeLa-S)	This study	N/A
UBE1	Boston Biochem	E-305
UBch5c	Boston Biochem	E2–627
RNase A	Invitrogen	12091–039
RNase H	NEB	M0297
Nuclease S1	Sigma	N5661
FastAP alkaline phosphatase	Thermo Fisher	EF0651
SUPERase•In RNase inhibitor	Thermo Fisher	AM2694

Reagent or Resource:	Source:	Identifier:
RNaseOut recombinant ribonuclease inhibitor	Thermo Fisher	10777019
RNase T1	Thermo Fisher	EN0542
Polynucleotide Kinase	NEB	B0201S
Protesase & phosphatase inhibitor cocktail	Thermo Fisher	A32961
Flag peptide	Sigma	F3290
Benzonase	Sigma	E1014
Anti-Flag M2 agarose beads	Sigma	A2220
Anti-Flag M2 magnetic beads	Sigma	M8823
Ni-NTA beads	Qiagen	88221
TUBE beads	Boston Biochem	AM-130
Ubiquilin-HALO beads	Zhao et al., 2018	N/A
TAB2-HALO beads	Zhao et al., 2018	N/A
Hoechst 33342	BD Bioscience	561908
Adenosine ribonucleoside	Cayman Chemical Company	21232
Guanosine 5’-monophosphate	Cayman Chemical Company	16957
Cytidine 5’-triphosphate	Cayman Chemical Company	18147
1-methyladenosine ribonucleoside	Cayman Chemical Company	16937
7-methylguanosine ribonucleoside	Cayman Chemical Company	15988
3-methylcytidine ribonucleoside	Cayman Chemical Company	21064
ProLong Gold	Invitrogen	P36930
PB (Pladienolide B)	Cayman Chemical Company	16538
Puromycin	Sigma	P8833
Hydroxyurea	Sigma	H8627
Bleomycin	Millipore-Sigma	203401
Shield-1	Takara Bio	632189
Doxycycline	Sigma	D3447
Methyl methanesulfonate (MMS)	Sigma	129925
Dimethyl sulfate (DMS)	Sigma	D2438
Camptothecin (CPT)	Selleckchem	S1288
Critical commercial assays		
MTS assay	Promega	G3580
Click-iT Nascent RNA Capture Kit	Thermo Fisher	C10365
Next Small RNA Library Prep Set for Illumina	NEB	7300
HiScribe T7 *In Vitro* Transcription Kit	NEB	E2050
RNA Clean & Concentrator-5 Kit	Zymo Research	R1013
RNasey Mini Kit	Qiagen	217004

Reagent or Resource:	Source:	Identifier:
Comet Assay	Trevigen	4250–050-K
ProtoScript First Strand cDNA Synthesis Kit	NEB	E6300
DNeasy Blood & Tissue Kit	Qiagen	69506
Nucleoside Digestion Mix	NEB	M0649S
Deposited Data		
Raw sequencing data	This study	GEO: GSE158090
Original data	This study	Mendeley Data: https://doi:10.17632/fmzn5hdbmw.1
Experimental models: Cell lines		
293T	ATCC	N/A
HeLa	ATCC	N/A
HeLa-S	ATCC	N/A
U2OS	ATCC	N/A
U2OS FUCCI	Byrum et al., 2019	N/A
U2OS ASCC2 KO	Brickner et al., 2017	N/A
U2OS ASCC3 KO	Brickner et al., 2017	N/A
U2OS 2–6-3	Janicki et al., 2004	N/A
U2OS 2–6-5	Shanbhag et al., 2010	N/A
U2OS ASCC3$^{G1354D/G1354D}$	This study	N/A
Oligonucleotides		
For PCR primers, see Table S7	IDT	N/A
m1A RNA substrate (for demethylase assay): 5’-CAGAGGAGGUAAAAA AAUGG[m1A]AUUGUACAAA-3’	Midland Certified Reagents Company	N/A
1meA DNA substrate (for demethylase assay): 5’-CAGAGGAGGUAAAAAAAUGG [1meA]AUUGUACAAA-3’	Midland Certified Reagents Company	N/A
RNA substrate (for methyltransferase assay): 5’-CAGAGGAGGUAAAAAAAUGGAAUUGUACAAA-3’	IDT	N/A
DNA substrate (for methyltransferase assay): 5’-CAGAGGAGGUAAAAA AAUGGAAUUGUACAAA-3’	IDT	N/A
Recombinant DNA		
pET-28a-Flag-BsV-AlkB-NLS	This study	N/A
pET-28a-Flag-BsV-AlkB-NLS (H156A)	This study	N/A
pHAGE-Flag-BsV-AlkB-NLS	This study	N/A
pHAGE-Flag-BsV-AlkB-NLS (H156A)	This study	N/A
pHAGE-3xHA-ASCC2	Brickner et al., 2017	N/A
pHAGE-Flag-METTL8-NLS	This study	N/A
pHAGE-Flag-METTL8-NLS (D230A)	This study	N/A
pHAGE-Flag-METTL8-NLS (G204A/G206A)	This study	N/A
pHAGE-Flag-TRMT61A-NLS	This study	N/A
pHAGE-Flag-TRMT61A-NLS (D181A)	This study	N/A
pDD-Flag-mCherry-LacI	This study	N/A

Reagent or Resource:	Source:	Identifier:
pDD-Flag-METTL8-NLS-mCherry-LacI	This study	N/A
pDD-Flag-METTL8-NLS-mCherry-LacI (G204A/G206A)	This study	N/A
pMSCV-Flag-HA-RNF113A (WT and RING mutants)	Brickner et al, 2017	N/A
pMSCV-Flag-HA-RNF113A (ZnF mutants)	This study	N/A
pHAGE-3xHA-RNF113A	Brickner et al, 2017	N/A
pHAGE-3xHA-RNF113A (ZnF mutants)	This study	N/A
T7-driven β-globin pre-mRNA	Movassat et al, 2014	N/A
pHAGE-Flag-TRMT61A (WT and catalytic dead)	This study	N/A
Software and algorithms		
OpenComet v1.3.1	OpenComet	N/A
ImageJ	ImageJ	N/A
Sequest	Eng et al., 1994	N/A
STAR v2.0.4b	Dobin et al., 2013	N/A
Subread:featureCount v1.4.5	Liao et al., 2014	N/A
Salmon v8.0.2	Patro et al., 2017	N/A
RseQC v2.3	Wang et al., 2012	N/A
Flexbar v3.5.0	https://github.com/seqan/flexbar	N/A
STAR v2.7.8	https://github.com/alexdobin/STAR	N/A
Bedtools v2.30.0	https://bedtools.readthedocs.io	N/A
Samtools v1.12	http://www.htslib.org	N/A
CLAM pipeline v1.2.0	https://github.com/Xinglab/CLAM	N/A
Homer v4.11	http://homer.ucsd.edu/homer/ngs/annotation.html	N/A